

OPTIMAL HARVESTING STRATEGY FOR *HAEMATOCOCCUS PLUVIALIS*
USING A STELLA-BASED MODEL

A THESIS SUBMITTED TO THE GRADUATE DIVISION OF THE
UNIVERSITY OF HAWAI'I PARTIAL FULFILLMENT
OF THE REQUIREMENTS FOR THE DEGREE OF

MASTER OF SCIENCE

IN

BIOENGINEERING

DECEMBER 2004

By
Shu Ki Tsang

Thesis Committee:

Stephen Masutani, Chairperson
Charles Kinoshita
Traci Sylva

ACKNOWLEDGEMENTS

I would like to acknowledge the financial support of the U.S. Department of Energy. Without their funding, this thesis would not have been possible.

I would also like to recognize the contributions of various people who made this thesis possible. Drs. Masutani, Kinoshita and Sylva, I would like to express my deepest gratitude to you for the support and guidance that you have provided throughout the last three and half years. Many thanks to Miguel Olaizola and his staff at Mera Pharmaceuticals, Inc. for providing data and samples for this project and for answering all of my questions. Dr. Gérard Nihous, thank you for your help in identifying appropriate relationships that were used in the model. Thanks to Charley Nelson, Dr. Loren Gautz and Ryan Kurasaki for your help in constructing the instruments used in the experiments. Ryan, thanks also for being a great office mate during this project. Thanks to Tersha Enriques for reorganizing the data that was used in the model. Dr. Liujuan Tang, thank you for sharing some of your Matlab expertise with me. Dr. Scott Turn, thank you for letting me borrow references and use the gas chromatograph. Dr. Wuyin Wang, thank you for showing me how to use the gas chromatograph. And to my best friend, Rowena Romano, thanks for the insight and advice about writing a master's thesis.

I want to thank a very special person in my life, my fiancée, Catherine Simonovich, for the numerous nights you stayed up late to edit my thesis. Also, thank you for the love, support, and encouragement that you have shown me in the past few years. From the bottom of my heart, thank you for everything.

Last but not least, I want to thank my parents for their patience and love over the years and for the sacrifices they made by bringing my siblings and I to Hawai‘i so we could have a chance for a better education in America.

ABSTRACT

One method for reducing the atmospheric concentration of carbon dioxide, CO₂, a greenhouse gas that plays a role in global warming, is to capture it from stationary combustion systems that burn fossil fuels and sequester it underground, in the deep ocean or in biological sinks such as photosynthetic microalgal species. The cost of capture and sequestration of CO₂ is not insignificant and this poses a serious hurdle to the implementation of this greenhouse gas emissions mitigation strategy. Toward this end, research and development is being conducted to develop low-cost, high efficiency CO₂ gas separation systems. Another alternative that has been explored is utilizing captured CO₂ in commercial processes to generate an offsetting income stream, while displacing CO₂ that would otherwise need to be generated (by oxidation of fossil carbon) for these processes.

Under adverse environmental conditions, the photosynthetic microalgae *Haematococcus pluvialis* produces a high-value compound called astaxanthin, a carotenoid pigment that provides health benefits to humans and that is also used in mariculture feed to enhance the color of salmon flesh. Mera Pharmaceuticals, Inc. has an industrial-scale astaxanthin production facility on the island of Hawai'i. In their production process, *Haematococcus pluvialis* is first grown in a photobioreactor called a Mera Growth Module (MGM). A portion of the culture is then transferred to open ponds where astaxanthin accumulates in the cells under imposed environmental stress. The harvesting strategy for the transfer of cells from the MGM to the pond has not been optimized.

The goal of this study was to explore utilization of captured CO₂ for *Haematococcus pluvialis* cultivation and to assess the benefits of this in terms of CO₂ displacement (utilization) and biomass production (*i.e.*, revenue generation). The specific objective of the research described in this thesis was to develop a process model that could be applied to optimize the harvesting strategy from the perspective of maximizing carbon uptake. The model employed STELLA, a commercially available simulation software package.

Results of the present study suggest that the carbon capture efficiency of the photobioreactor system is modest. About 25% of the carbon sparged into the media is eventually assimilated into the cell biomass. Most of the remaining 75% is lost via degassing and venting. To maximize carbon capture efficiency, a closed system in which vented gas is recirculated back into the photobioreactor should be explored.

Simulations were conducted to identify harvesting scenarios that would maximize cell biomass yield (and, hence, carbon capture). It was determined that reducing harvesting quantities while increasing target cell concentrations in the photobioreactor could provide significant increases in cumulative yield (about 10%) compared to the harvesting strategy currently applied by Mera Pharmaceuticals, Inc. Unfortunately, this would require daily harvests and additional ponds. A target cell concentration of 5.5×10^5 cells/mL and a harvesting cell quantity of 3.2×10^{12} cells produced a realistic (*i.e.*, achievable with the current labor force and ponds) maximum cumulative yield of 3.12×10^{13} cells, which is 2.57×10^{11} cells greater than the cumulative yield of the current harvesting strategy. This is an insignificant gain; hence, the current harvesting strategy

appears to be very close to the best scenario under the real constraints imposed by labor force and available ponds.

Although the number of harvesting scenarios tested was limited, the results suggest that the process model can be a valuable tool in optimizing microalgae production operations from the perspective of profit or carbon capture.

TABLE OF CONTENTS

ACKNOWLEDGEMENTS	iii
ABSTRACT.....	v
LIST OF TABLES	xi
LIST OF FIGURES	xii
CHAPTER 1. INTRODUCTION	1
1.1. Objectives	5
CHAPTER 2. BACKGROUND.....	7
2.1. Anthropogenic Carbon Dioxide Emissions	7
2.2. Carbon Sequestration Using Microalgae	10
2.3. <i>Haematococcus pluvialis</i>	13
2.4. Astaxanthin	14
2.5. Large-scale Astaxanthin Production Process.....	15
CHAPTER 3. METHODS AND PROCEDURES	17
3.1. <i>Haematococcus pluvialis</i> Production Process in the MGM	18
3.2. Carbon Mass Balance	20
3.2.1. <i>Evaluation of Terms of the Carbon Mass Balance</i>	21
3.2.2. <i>Carbon Venting from the MGM</i>	23

3.2.2.1. ORIFICE FLOW METER.....	23
3.2.2.2. GAS SAMPLING AND ANALYSIS.....	24
3.2.2.3. GAS VENTING EXPERIMENTS	25
3.2.3. <i>Carbon Bound in Biomass</i>	27
3.2.4. <i>Change in Carbon Concentration in the Headspace</i>	28
3.2.5. <i>Relationships Between Variables in the Carbon Mass Balance Equation</i>	29
3.3. <i>Haematococcus pluvialis</i> Population.....	30
3.4. Harvesting Strategy.....	31
3.5. STELLA Model	31
3.6. Model Verification.....	32
3.7. Sensitivity Analysis	32
3.8. Model Simulations.....	33
CHAPTER 4. RESULTS AND DISCUSSION.....	34
4.1. Carbon Venting Rates from the MGM	34
4.2. Carbon Assimilated by Biomass.....	36
4.3. Carbon Mass Balance Calculations	38
4.4. Process Model Relationships	43
4.5. STELLA Process Model.....	47
4.6. Verification of the STELLA Model.....	48
4.7. Sensitivity Analysis	50

4.8. Model Simulations.....	51
CHAPTER 5. SUMMARY AND CONCLUSIONS.....	54
APPENDIX A. PHOTOGRAPHS.....	56
APPENDIX B. STELLA MODEL.....	59
REFERENCES.....	60

LIST OF TABLES

Table 2.1. High-Value Products from Microalgae (Molina Grima <i>et al.</i> , 1999)	11
Table 3.1. <i>Haematococcus Pluvialis</i> Samples	28
Table 4.1. Vent Flow Rate and Vented Carbon Concentration from MGM.....	34
Table 4.2. Mass Flow Rate of Vented Carbon from MGM.....	35
Table 4.3. Dry Cell Mass and %TOC for <i>Haematococcus pluvialis</i> Samples	37
Table 4.4. Carbon Mass Balance for MGM.....	39
Table 4.5. Comparison of Model Results and Data for MGM M10-040810	48
Table 4.6. Percent Error of Model Predictions of Cell Population for M10-040810	49
Table 4.7. Target Cell Concentration and Cumulative Yield from the Sensitivity Analyses	50
Table 4.8. Harvesting Quantity and Cumulative Yield from the Sensitivity Analyses ...	51
Table 4.9. Target Cell Concentration, Harvest Quantity, and Maximum Cumulative Yield for Six Scenarios	52

LIST OF FIGURES

Figure 1.1. Recovery and sequestration of carbon dioxide from stationary combustion systems by photosynthesis of microalgae (from Nakamura & Senior, 2001).	3
Figure 4.1. Mass of carbon per cell.....	38
Figure 4.2. Nighttime headspace CO ₂ concentration for 4/26/03.....	42
Figure 4.3. Nighttime headspace CO ₂ concentration for 4/27/03.....	42
Figure 4.4. Daily carbon mass flow rate injected into the MGM over time.	44
Figure 4.5. Daily carbon mass flow rate degassed out of the media vs. daily carbon mass flow rate injected into the MGM.....	45
Figure 4.6. Daily change in the mass of carbon bound in biomass vs. daily change in the mass of total carbon in the media.	46
Figure 4.7. Daily specific growth rate vs. daily rate of carbon assimilation.	47
Figure 4.8. Comparison of model results and data for MGM M10-040810.....	49
Figure A.1. Photograph showing the front view of a MGM photobioreactor.	56
Figure A.2. Photograph showing the side view of a MGM photobioreactor.....	56
Figure A.3. Photograph showing the orifice meter and the connector piece.....	57
Figure A.4. Photograph of the gas sampling system.	57
Figure A.5. Photograph showing the gas sampling system and the orifice meter attached to the photobioreactor vent at Mera Pharmaceuticals' facility.	58
Figure A.6. Photograph of the of the Shimadzu Model 14A gas chromatography.	58
Figure B.1. Completed STELLA model.....	59

CHAPTER 1. INTRODUCTION

The majority of anthropogenic CO₂ emissions results from the burning of fossil fuels for energy production (IPCC, 2001; Nakamura & Senior, 2001). Increased global energy demand, especially in developing countries, will cause CO₂ emissions to grow in the near future. The projected increase in CO₂ emissions will lead to continued accumulation of this gas in the atmosphere, resulting in serious environmental effects due to global warming and climate changes (Ramanathan, 1999). These concerns have prompted scientists worldwide to consider options for minimizing future increases in the atmospheric CO₂ concentration (Palumbo *et al.*, 2004).

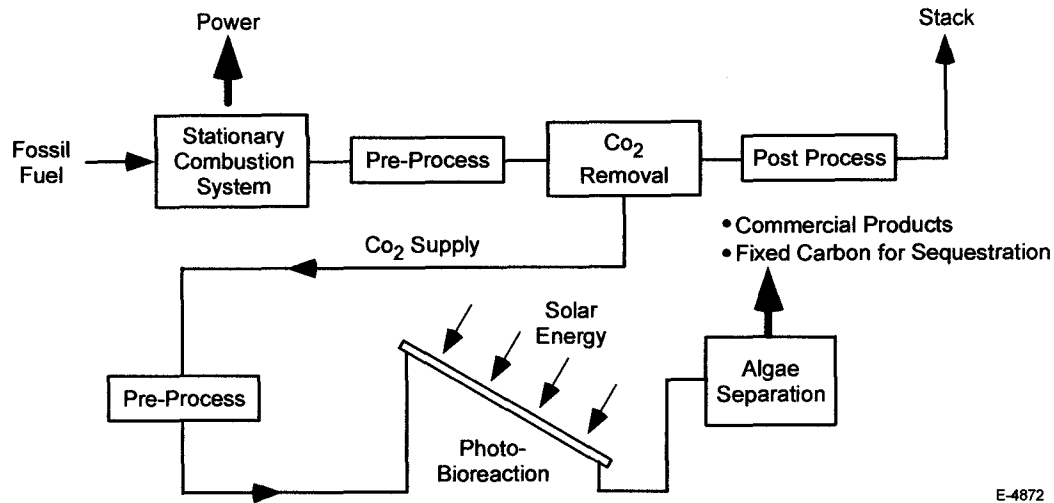
One possible option to mitigate CO₂ emissions is to sequester “fossil” carbon (Kim & Edmonds, 2000; U.S. Department of Energy, 2004). Carbon sequestration involves capturing CO₂ emitted from fossil fuel combustors and storing it away from the atmosphere, either underground, in the deep ocean, or in long-term biological sinks. The present study focuses on the biological capture of CO₂.

Photosynthesis is a process that autotrophs use to capture and store carbon. Aquatic microalgae are considered to be one of the fastest growing autotrophs in the world whose carbon fixing rates are higher than those of terrestrial plants by one order of magnitude (Nakamura & Senior, 2001; Olaizola, 2000). Microalgal photosynthesis may therefore represent a possible method for capturing anthropogenic CO₂ from combustor flue gases (Olaizola, 2004). While microalgal culturing is expensive, certain species of microalgae can produce high value commercial products, such as β -carotene and

fucoxanthin, that would offset carbon sequestration costs (Olaizola, 2004; Nakamura & Senior, 2001).

The duration of carbon sequestration by microalgal photosynthesis can vary widely, depending on whether the carbon is ultimately mineralized and deposited or consumed and respired by other organisms. On the other hand, commercial cultivation of microalgae for high value products requires the addition of CO₂ which is usually purchased from an industrial gas supplier. It has been argued that utilization of CO₂ from fossil fuel combustor flue gases for microalgae cultivation effectively displaces the industrial CO₂ source, reducing total atmospheric CO₂ emissions.

Physical Sciences Inc., Mera Pharmaceuticals, Inc., and the Hawai'i Natural Energy Institute of the University of Hawai'i at Mānoa currently are working jointly on a research program funded by the U.S. Department of Energy to develop technologies for the capture and sequestration of CO₂ from stationary combustion systems based on photosynthetic microalgae (Nakamura & Senior, 2001). Figure 1.1 shows the general approach being investigated where CO₂ from flue gas is added to a photobioreactor containing photosynthetic microalgae which convert it into high-value compounds or mineralized carbon.



E-4872

Figure 1.1. Recovery and sequestration of carbon dioxide from stationary combustion systems by photosynthesis of microalgae (from Nakamura & Senior, 2001).

The microalgal species selected for this project is *Haematococcus pluvialis*, a green unicellular freshwater biflagellate (Margalith, 1999). Under adverse environmental conditions such as high irradiance and nitrogen deprivation, *Haematococcus pluvialis* produces a high-value carotenoid pigment, astaxanthin, that is an antioxidant and blocks UV light. Astaxanthin has been touted as having anti-inflammatory properties and numerous other health benefits for humans (Fábregas *et al.*, 2001; Guerin *et al.*, 2002). Although astaxanthin can be synthesized from various hydrocarbons as an additive to fish feed (to enhance the color of salmon flesh) for aquaculture, nutraceutical grade astaxanthin is usually produced using *Haematococcus pluvialis*.

Mera Pharmaceuticals, Inc. has developed and operated an industrial-scale astaxanthin production facility located at the Natural Energy Laboratory Hawai'i Authority (NELHA) on the west coast of the island of Hawai'i. In their process, *Haematococcus pluvialis* biomass production occurs in a Mera Growth Module (MGM),

a closed photosynthetic bioreactor (Mera Pharmaceuticals, Inc., 2003a; Olaizola, 2000). The purpose of using an MGM is to maximize the production of *Haematococcus pluvialis* while reducing the risk of contamination (Olaizola, 2000). A small portion of culture in the MGM is harvested periodically according to a harvesting strategy. The harvested cells are transferred to an open pond system where astaxanthin accumulation occurs under imposed environmental stress (increased light exposure, heating, and nutrient deprivation). The harvesting strategy is based on meeting two criteria: (1) a specific number of cells needed to inoculate the open ponds and (2) a minimum cell concentration in the MGM that must be achieved before harvesting.

Harvesting strategies are commonly used in managing aquaculture operations. Aquaculture industries, such as shrimp production, have conducted extensive studies to optimize harvesting strategies. A harvesting strategy is a quantitative tool that is used to determine optimal management practices so a facility can maximize profit (Leung *et al.*, 1989). Key components of a harvesting strategy include knowledge about the biological, physical and economic elements of the production process.

Two primary considerations in assessing the value and effectiveness of CO₂ capture and sequestration by commercial microalgal cultivation are carbon capture efficiency and the generation of an income stream to offset capital and operating costs. In the MGM, CO₂ is used as a primary carbon source for cell biomass production and to control media pH. Only a fraction of the CO₂ sparged into the photobioreactor is assimilated into the biomass pool; most of the added CO₂ is eventually discharged from the MGM.

Based on past aquaculture results, there is reason to believe that carbon capture and revenues could be improved by optimizing the harvesting strategy. Toward this end, a model of the Mera process was developed, applying principles similar to the ones used in the aquaculture industry, to investigate the effects of modifying the harvesting strategy on CO₂ utilization and cell production.

An optimized harvesting strategy for the large-scale production of microalgae is a new concept in microalgal modeling. Past microalgal models predicted culture growth rate as a function of light intensity, light/dark cycle effects induced by cell position in the depth of the culture, average solar irradiance, or non-limiting nutrients (Csögör *et al.*, 1999; Molina Grima *et al.*, 1996; Pruvost *et al.*, 2002; Zonneveld, 1996).

In addition to the value that an optimal harvesting strategy would provide to the present DOE research project, the process model could serve as a template for carbon sequestration using other microalgal species.

1.1. Objectives

The objective of this study is to optimize the harvesting strategy for the production of *Haematococcus pluvialis* to maximize carbon capture. The approach taken to attain this objective comprised the following activities:

- Develop and verify a model that accurately depicts the *Haematococcus pluvialis* production process in the MGM.
- Apply the model to simulate and quantitatively evaluate different harvesting strategy scenarios.

- Identify the harvesting strategy that will provide the maximum carbon capture by *Haematococcus pluvialis*.

CHAPTER 2. BACKGROUND

This chapter provides a general discussion of the problem of increasing anthropogenic CO₂ emissions and the mitigation strategy based on carbon sequestration using microalgae. Background information on *Haematococcus pluvialis*, astaxanthin production, and other topics relevant to the research described in this thesis also are included.

2.1. Anthropogenic Carbon Dioxide Emissions

Emissions of CO₂, due in large part to the burning of fossil fuels for energy production, have increased significantly since the mid 1800s (Palumbo *et al.*, 2004; IPCC, 2001). Before 1863, anthropogenic emissions from fossil fuel did not surpass 0.1 gigatons of carbon per year (GtC/year), but by 1995, those emissions had reached 6.5 GtC/year (Wuebbles *et al.*, 1999). As a result of the increase in anthropogenic CO₂ emissions, data collected at the Mauna Loa Observatory in Hawai‘i indicate that the yearly average atmospheric CO₂ concentration has risen from 316 parts per million by volume (ppmV) in 1959 to 364 ppmV in 1997 (Wuebbles *et al.*, 1999).

Emissions of anthropogenic CO₂ and other greenhouse gases may have contributed to the current warming trend. The earth’s surface temperature has increased approximately 0.65° C from 1851 to 1995. Rising levels of atmospheric greenhouse gas have also been implicated as the cause of other observed environmental changes such as the decrease in annual snow cover in the Northern Hemisphere, increasing Antarctic snowfall, and rising sea levels (Wuebbles *et al.*, 1999).

Anthropogenic CO₂ emissions are expected to continue to accelerate during this century in concert with the growing demand for energy worldwide (Palumbo *et al.*, 2004; IPCC, 2001). Energy demand has been predicted to increase by 1.3% per year in industrialized nations and by up to 9.2% annually in developing nations (Kessel, 2000). Currently, fossil fuels provide for about 90% of the global energy demand, and high levels of consumption of this resource will probably continue in the immediate future. Atmospheric CO₂ concentrations will rise accordingly, and may reach levels of between 600 to 900 ppmV by the year 2050.

Accumulation of CO₂ and other greenhouse gases in the atmosphere will alter the albedo and affect the radiative energy budget of the earth. Average global temperatures are predicted to rise by 1.0 to 3.5° C over the next 50 to 100 years (Palumbo *et al.*, 2004) although these changes will not be uniformly distributed. Other aspects of climate, such as precipitation, may also change dramatically.

The impacts of climatic change on humanity and ecosystems could be manifold and significant. As the average global temperature increases, Antarctic ice caps and glaciers will melt, causing the sea level to rise. It is predicted that mean sea level could increase by 15 to 95 cm in the next 100 years (Neff, 1999). Rising sea levels will threaten low lying islands and coastal zones. Currently, between 50 and 70 percent of the world's human population resides in coastal zones (Neff, 1999).

Elevated mortality rates from heat waves are another possible consequence of global warming. Studies in selected cities in North America, North Africa, and East Asia show that the number of heat-related deaths could double in the next 100 years, representing several thousand extra deaths annually in various large cities (U.S. Climate

Action Network, 1996). In addition to growing numbers of heat-related deaths, it is predicted that cases of infectious tropical diseases such as malaria will increase as the range of their vectors expands (U.S. Climate Action Network, 1996). Currently, about 45% of the world population is at risk of contracting malaria. This percentage may increase to around 60% by 2070 (Buchdahl *et al.*, 2002).

Global warming could influence agriculture because the limiting factors of crop growth are temperature and rainfall (Buchdahl *et al.*, 2002). Water resources would also be impacted since precipitation patterns could shift dramatically.

The gravity of the potential impacts of greenhouse gas-induced climatic change has prompted scientists worldwide to develop strategies to mitigate CO₂ emissions (Palumbo *et al.*, 2004). These strategies include conservation, improved energy efficiency, and a shift to nuclear power or renewable energy systems. Another option that addresses the continued use of fossil fuels in the foreseeable future is to capture CO₂ from the exhaust streams of large stationary combustion systems and sequester it from the atmosphere underground, in the deep ocean, or in biological sinks

Sequestration is a controversial approach that is generally not endorsed by environmental groups since it is perceived to perpetuate, rather than phase out, the use of fossil fuels. Nonetheless, studies have indicated that it could be an effective interim means to control greenhouse gas emissions while alternative energy systems are being developed and integrated into the energy infrastructure. While technologies to capture and sequester CO₂ exist, the associated costs of systems using these current technologies are significant and the magnitude of the benefits and risks of sequestration have not been clearly established.

2.2. Carbon Sequestration Using Microalgae

Three potential sinks have been proposed to sequester CO₂ from fossil fuel combustion systems: underground, in the deep ocean, or in biological carbon pools such as terrestrial plants, phytoplankton, and microalgae. Among the possible biological carbon reservoirs, photosynthetic microalgae systems are an attractive option since their carbon fixing rates are high, certain species can be marketed to generate an income stream to offset the cost of CO₂ capture, and cultivation facilities can be directly integrated into the flue gas clean-up flow train.

Photosynthesis by terrestrial plants proceeds too slow to effectively offset the point source emissions of CO₂ within a confined area (Nakamura & Senior, 2001). Aquatic microalgae, on the other hand, are one of the fastest growing autotrophs in the world and their carbon fixing rates are higher than those of terrestrial plants by one order of magnitude (Olaizola, 2000). While microalgal culturing is expensive, certain microalgae produce high commercial value products. Table 1.1 provides examples of high-value products from microalgae.

Table 2.1. High-Value Products from Microalgae (Molina Grima *et al.*, 1999)

Product	Source Organism	Current or Potential Use
Amphidinolides and amphidinins	<i>Amphidinium</i> sp.	Antitumor agent
Astaxanthin	<i>Haematococcus pluvialis</i> , <i>Chlorella</i> sp.	Pigment
β -Carotene	<i>Dunaliella</i>	Colorant, food supplement
Docosahexaenoic Acid	<i>Isochrysis galbana</i>	Essential fatty acid
γ -Linolenic acid	<i>Spirulina</i> sp.	Essential fatty acid
Other polyunsaturated fatty acids	<i>Phaeodactylum tricornutum</i> , <i>Isochrysis galbana</i>	Health care, food supplement
Fucoxanthin	<i>Phaeodactylum tricornutum</i>	Antioxidant
Goniodominas	<i>Alexandrium hiranoi</i>	Antifungal agent
Oscillapeptin	<i>Oscillatoria agardhii</i>	Elastase inhibitor
Phycobiliproteins	Red algae, cyanobacteria	Colorants
Phycocyanin	<i>Spirulina platensis</i>	Colorant

Capture of CO₂ from stationary combustion systems by microalgal photosynthesis may be accomplished by flowing flue gas into a photobioreactor where photosynthetic microalgae convert the CO₂ into high-value compounds or mineralized carbon.

Advantages of this approach are: (1) high purity CO₂ gas is not required for microalgal culture (*e.g.*, flue gas containing 2-5% CO₂ is sufficient for microalgal culture); (2) other compounds in the flue gas such as NO_x or SO_x might serve as nutrients for the microalgae; (3) microalgae-produced high value products could offset the capital and operating costs of the process; and (4) the process could have minimal negative impacts on the environment.

There are a number of factors that must be considered in culturing microalgae. Microalgal monoculture must be maintained to prevent other microorganisms from competing with the monoculture to achieve maximum production of the specific high commercial value product (Olaizola, 2004). The best solution to maintaining a

microalgal monoculture is to use enclosed photobioreactors. Open systems, such as ponds, can only be used with species of microalgae such as *Dunaliella* and *Spirulina*, that have the ability to survive harsh environments that exclude other contaminant species. Microalgal light utilization must be maximized and photoinhibition must be minimized by controlling the culture optical depth, a function of the physical culture depth and cell density, or by changing the microalgal light harvesting apparatus. Finally, transfer of CO₂ gas to the culture, a function of flue gas composition and medium pH and alkalinity, must be maximized. CO₂ gas dissolved in the culture medium, may be assimilated by the microalgae or degassed out of the liquid phase into the gas phase (Olaizola, 2004).

Production methods have been developed for commercial culturing of certain strains of microalgae. These methods generally reflect the objective of maximizing profits rather than carbon capture. The potential for CO₂ sequestration using microalgae was the focus of a major research program sponsored by the Japanese government and administered by the Research Institute of Technology for the Earth (RITE) (Masutani & Nakamura, 1999). RITE spent \$117 million in the area of biological CO₂ fixation and utilization between fiscal year (FY) 1990 and FY 1999 (Masutani & Nakamura, 1999). This program funded a host of projects including CO₂ fixation using microalgae possessing the capacity to tolerate environmental extremes and development of photobioreactors for CO₂ fixation.

In 2001, Physical Sciences Inc., Mera Pharmaceuticals, Inc., and the Hawai'i Natural Energy Institute of the University of Hawai'i at Mānoa initiated a joint research project funded by the U.S. Department of Energy to quantify the efficacy of industrial-

scale, microalgae-based carbon sequestration systems. This study focused on production of *Haematococcus pluvialis* using a process developed by Mera Pharmaceuticals, Inc.

2.3. *Haematococcus pluvialis*

Haematococcus pluvialis is a green unicellular freshwater biflagellate (Margalith, 1999). The cells of *Haematococcus pluvialis* range from spherical to elliptical and are surrounded by a cell wall, having inner and outer diameters of approximately 34 μm and 37.5 μm , respectively (Iyengar & Desikachary, 1981). The cells are composed of starch and haematochrome, and the cells contain cup-shaped chloroplasts.

The life cycle of *Haematococcus pluvialis* consists of four cell stages: vegetative cell growth, encystment, maturation, and germination (Kobayashi *et al.*, 1997). The duration of the life cycle is two weeks. During the vegetative cell growth stage, green flagellate cells are mobile in a growth medium and reproduction occurs by cell division (Margalith, 1999). The medium consists of 14.6 mM sodium acetate, 2.7 mM L-asparagine, 2.0 g/L yeast extract, 0.985 mM $\text{MgCl}_2 \cdot 6\text{H}_2\text{O}$, 0.036 mM $\text{FeSO}_4 \cdot 7\text{H}_2\text{O}$, 0.135 mM $\text{CaCl}_2 \cdot 2\text{H}_2\text{O}$, and deionized water (Kobayashi *et al.*, 1991).

Under adverse environmental conditions such as high irradiance and nitrogen deprivation, cells are immobilized by shedding their flagella, and green vegetative cells are transformed into brown immature cyst cells throughout the encystment stage (Fábregas *et al.*, 2001; Kobayashi *et al.*, 1997; Margalith, 1999; Olaizola, 2000). The cyst cells are called aplanospores. During the maturation stage, the brown aplanospores are enlarged with a thicker cell wall and the aplanospores' color changes to red. This red

color signifies the accumulation of astaxanthin (Margalith, 1999). At the end of the maturation stage, over 90% of the carotenoids in the aplanospores are composed of astaxanthin. In a fresh medium, mature cysts release daughter cells and leave behind the cell wall throughout the germination stage (Kobayashi *et al.*, 1997; Margalith, 1999).

2.4. Astaxanthin

Astaxanthin is an oxygenated carotenoid pigment that is a fat-soluble nutrient with a molecular weight of 596.8 Da (Beta Immune, 2004). The structure of astaxanthin is a long, polyene chain with a six-membered ring polar group on each end.

Haematococcus pluvialis is one of the natural sources of highly concentrated astaxanthin, containing 1.5-3.0% astaxanthin by dry weight (Lorenz & Cysewski, 2000). Other natural sources of astaxanthin include krill oil and meal, crawfish oil, and *Phaffia* yeast, but they contain lower astaxanthin concentrations ranging from 0.15% astaxanthin by dry weight in the oils to 0.40% astaxanthin by dry weight in the yeast.

Astaxanthin is well-known for enhancing the pinkish-red tone in the flesh of salmon, shrimp, lobsters, and crayfish (Lorenz & Cysewski, 2000). These animals are unable to synthesize astaxanthin so astaxanthin must be supplied in their diet. In aquatic organisms in which astaxanthin is found, it has a variety of crucial biological functions, ranging from protection against UV light and oxidation of polyunsaturated fatty acids to pigmentation (Guerin *et al.*, 2002).

Research has been conducted to determine the possible effects of astaxanthin on human health. In laboratory and animal models, studies have demonstrated that

astaxanthin may provide health benefits to humans, such as stimulation of immune system response factors, anti-cancer properties, protection of tissues against ultraviolet light damage and photo-oxidation, anti-inflammatory effects, and prevention of oxidative damage to blood LDL-cholesterol (Mera Pharmaceuticals, Inc., 2004).

2.5. Large-scale Astaxanthin Production Process

Mera Pharmaceuticals, Inc., formerly known as Aquasearch, is one of few companies that operate large-scale astaxanthin production processes. The company has developed a variety of systems for astaxanthin production (Olaizola, 2000). For industrial-scale biomass production of *Haematococcus pluvialis*, the Mera Growth Module (MGM), a closed photosynthetic bioreactor system, is utilized (Mera Pharmaceuticals, Inc., 2003a; Olaizola, 2000). The purpose of using a MGM is to produce large quantities of fast-growing *Haematococcus pluvialis* culture with minimal risk of contamination (Olaizola, 2000). The MGM is composed of plastic tubes occupying an area of 100 m² that are exposed to sunlight. Sunlight is the main factor controlling the biomass productivity of *Haematococcus pluvialis* (Molina Grima *et al.*, 1999; Olaizola, 2000).

Other key system components besides the MGM are needed for astaxanthin production. One component is an airlift that creates turbulence in the MGMs to keep cells from settling and to enhance desorption of photosynthetically generated oxygen through a gas-liquid interface (Olaizola, 2000; Weissman *et al.*, 1988). Another key component is a cooling system that controls temperature inside the MGM. At the

NELHA facility, temperature control is accomplished by immersing the MGM in a shallow pool of cold deep seawater. Other components include the CO₂ supply system that sparges measured quantities of industrial grade CO₂ gas into the liquid media contained in the MGM to control pH and supply necessary carbon, and a data acquisition and control system that monitors and controls conditions such as light, temperature, and nutrient concentration in the MGM (Mera Pharmaceuticals, Inc., 2003b).

A small portion of the *Haematococcus pluvialis* culture in the MGM is harvested periodically. The harvested cells are transferred to an open pond system where astaxanthin accumulation occurs (Olaizola, 2000). The pond's function is to induce astaxanthin accumulation in the *Haematococcus pluvialis* cells by creating adverse environmental conditions such as high irradiance (*i.e.*, solar irradiance can reach 2000 $\mu\text{mol photon m}^{-2} \text{ s}^{-1}$ at noon in the pond) and nitrogen deprivation. Green vegetative cells from the MGM are eventually transformed into red aplanospores that accumulate astaxanthin in the pond in about six days (Fábregas *et al.*, 2001; Olaizola, 2000). A paddlewheel is used to provide turbulence for cell mixing and cell suspension so all cells are exposed to high irradiance (Olaizola, 2000).

After the ponds are harvested, the astaxanthin is recovered. First, the microalgal cells are separated from the water through passive settling and then concentrated through centrifugation. The concentrated cells are ruptured using a high pressure homogenizer. The ruptured material is dried to concentrate the astaxanthin and the astaxanthin is packaged and sold (Olaizola, 2000).

CHAPTER 3. METHODS AND PROCEDURES

This Chapter summarizes the methods and procedures used to conduct the present modeling study and a few related experiments. As stated in Chapter 1, the objective of the study described in this thesis was to optimize the harvesting strategy for the industrial-scale production of *Haematococcus pluvialis* to maximize carbon capture. The key element in attaining this objective was the development of a process model that accurately simulates the partitioning of added CO₂ into the different carbon pools.

The procedure that was followed to develop the model and optimize the harvesting strategy included: (1) determining functional relationships for the dependence of *Haematococcus pluvialis* population in the MGM on the various operating parameters using the operational data provided by Mera Pharmaceuticals, Inc. or obtained experimentally; (2) employing these relationships to synthesize a process model based on the STELLA biological systems simulation software; (3) verifying the model by comparison with MGM operational data; (4) conducting analyses to determine the sensitivity of quantity of carbon captured by *Haematococcus pluvialis* to variations in the target cell concentration and the harvesting cell quantity; (5) applying the model in parametric studies to identify the target cell concentration and the harvesting cell quantity that provides maximum carbon capture by *Haematococcus pluvialis*.

Mera Pharmaceuticals, Inc. provided data from the operation of its MGMs identified as M13A-030423 and M10A-040810. The data included records of pH and temperature of the media, CO₂ injection, and information about the sampling and harvesting of *Haematococcus pluvialis*. The data from M13A-030423 included values of

media alkalinity measured each morning and alkalinity during the nights for the first few days of operation of the MGM. The pH data set comprised measurements of media taken every minute for M13A-030423 and every five minutes for M10A-040810. The temperature data set included measurements of media taken every five minutes for M10A-040810 and every fifteen minutes for M13A-030423. The CO₂ data set consisted of injection times and volumetric flow rate of the CO₂ injection stream. The cell sampling data set comprised sampling times and cell concentrations (typically three replications of each sample) and the harvesting data included the volumes of harvested microalgae and media and the corresponding dates and times.

3.1. *Haematococcus pluvialis* Production Process in the MGM

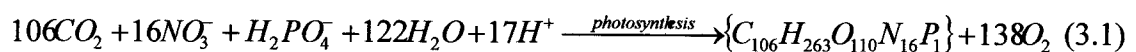
Photographs of the front and side views of the MGM that was employed in this study are provided in Figure A.1 and Figure A.2 in Appendix A, respectively. The MGM is a flexible cylindrical tube constructed from polyethylene and the end assemblies are made of polyvinyl chloride. Typically, the MGM has a volume of 25,000 L and occupies an area of 100 m². However, M13A-030423, the MGM that was used in the development of the model, had a volume of 16,500 L.

M13A-030423 was inoculated with *Haematococcus pluvialis* cells in a liquid growth media to about two-thirds of the MGM volume (about 11,000 L). The other one-third of the MGM volume (5,500 L), served as the gas headspace. *Haematococcus pluvialis* cells absorbed visible sunlight that provided the energy to convert inorganic materials (*e.g.*, CO₂, water, and mineral salts) to biomass (*i.e.*, additional cells) and

oxygen via photosynthesis (Dugan, 1980). Pure CO₂ gas was injected periodically into the MGM. A data acquisition and control system monitored and controlled the CO₂ injections along with the pH of the media (Mera Pharmaceuticals, Inc., 2003b).

Since CO₂ is an acid gas, consumption of CO₂ dissolved in the liquid media during photosynthesis increased the media pH. When media pH exceeded a user selected value, system controls triggered the injection of pure CO₂ gas into the liquid that was used to adjust the pH of the liquid. Once the media pH decreased to within the set operating range, the injection was automatically terminated. CO₂ injected into the MGM either dissolved in the media and was available for consumption by the cells or degassed out of the media into the headspace, where it could exit the MGM via a venting system. CO₂ was also added to the MGM by the airlift system employed to prevent cell settling and to enhance desorption of O₂. Ambient air pumped into the MGM contains low concentrations (about 380 ppmV) of CO₂.

Photosynthetic uptake of CO₂ produced an increase in pH of the liquid but did not increase the alkalinity (Nakamura *et al.*, 2004). On the other hand, other growth processes, such as the uptake of NO₃⁻ and H₂PO₄⁻, did increase the alkalinity based on Equation 3.1 below. The stoichiometry of photosynthesis-based cellular growth indicated that for every 106 moles of CO₂ taken up, 16 moles of NO₃⁻ and 1 mole H₂PO₄⁻ are consumed. Simultaneously, 17 moles of H⁺ are removed from the liquid which results in an equivalent increase in alkalinity (Nakamura *et al.*, 2004).



As the population of *Haematococcus pluvialis* in the MGM increased via photosynthesis, an average of 5,500 L of liquid containing an average of 3.2 trillion cells was harvested periodically and transferred to the open ponds to be stressed and to produce astaxanthin. Fresh media was added to the MGM after harvesting to compensate for the liquid removed.

3.2. Carbon Mass Balance

CO₂ was the primary carbon source for cell biomass production. CO₂ injected into the MGM was partitioned between the biomass, media, and the gas headspace of the MGM. The carbon balance relationship for the MGM is:

$$C_{in} - C_{out} = V_l M_C \left(\frac{d[C_{biomass}]}{dt} + \frac{d[DIC]}{dt} \right) + V_g M_C \left(\frac{d[C_{headspace}]}{dt} \right) \quad (3.2)$$

where C_{in} is the daily mass flow rate of carbon from both CO₂ and air injections into the MGM (g/day), C_{out} is the daily mass flow rate of carbon out of the MGM via venting (g/day), V_l is the volume of the media (L), M_C is the atomic weight of carbon (g/mol), $\frac{d[C_{biomass}]}{dt}$ is the daily rate of change in concentration of carbon bound in the biomass in the media (mol/L/day), $\frac{d[DIC]}{dt}$ is the daily rate of change in dissolved inorganic carbon concentration (mol/L/day), V_g is the volume of the headspace in the MGM (L), and

$\frac{d[C_{\text{headspace}}]}{dt}$ is the daily rate of change in carbon concentration in the headspace (mol/L/day).

3.2.1. Evaluation of Terms of the Carbon Mass Balance

Several of the terms in the carbon mass balance Equation 3.2 could be determined from operational data provided by Mera Pharmaceuticals, Inc.

The first term on the left hand side of Equation 3.2, C_{in} , the daily mass flow rate of carbon from both CO₂ and air injections into the MGM, was estimated from data on CO₂ and air injections. CO₂ injection data included the frequency, duration, and volumetric flow rate of the injections of pure CO₂. The mass of carbon injected as CO₂ per day could be calculated from this information. Air containing about 0.038% CO₂ by volume was injected into the MGM every minute, and the volumetric flow rate of the air was recorded. These data were used to calculate the mass flow rate of carbon transported into the MGM with the air.

Another term that could be estimated from operational data on alkalinity, pH, and media temperature was the daily rate of change in dissolved inorganic carbon concentration, $\frac{d[DIC]}{dt}$. Dissolved inorganic carbon (DIC) is the sum of carbonic acid, bicarbonate, and carbonate in the aqueous solution (LOICZ IGBP, 2000). DIC, along with total alkalinity and temperature, describe the CO₂ chemical system in freshwater media (LOICZ IGBP, 2000). The relationship for dissolved inorganic carbon is:

$$[DIC] = \left(\frac{TA + [H^+] - \frac{K_w}{[H^+]}}{\frac{[H^+]}{K_2} + 2} \right) \left(1 + \frac{[H^+]}{K_2} + \frac{[H^+]^2}{K_1 K_2} \right) \quad (3.3)$$

where [DIC] is the inorganic carbon concentration in meq/L, TA is the total alkalinity in meq/L, $[H^+]$ is the hydrogen ion activity (*i.e.*, $10^{-\text{pH}}$), K_w is the acid dissociation constant of water, K_1 is the first apparent dissociation constant for carbonic acid in water, and K_2 is the second apparent dissociation constant for carbonic acid in water.

Values of the dissociation constant of water and first and second dissociation constants can be determined from the following equations (Millero, 1979; UNESCO 1987) if the temperature of the media, T (K), is known:

$$K_w = e^{\left(148.9802 - \frac{13847.29}{T} - 23.6521 \ln T \right)} \quad (3.4)$$

$$K_1 = 10^{-\left(\frac{6320.81}{T} - 126.3405 + 19.568 \ln T \right)} \quad (3.5)$$

and

$$K_2 = 10^{-\left(\frac{5143.69}{T} - 90.1833 + 14.613 \ln T \right)} \quad (3.6)$$

Operational data provided by Mera Pharmaceuticals, Inc. were not sufficient to evaluate the terms C_{out} , $\frac{d[C_{biomass}]}{dt}$, and $\frac{d[C_{headspace}]}{dt}$ in the carbon mass balance. This required additional analysis and experiments.

3.2.2. Carbon Venting from the MGM

Mera Pharmaceuticals does not monitor the venting rate nor composition of the gas discharged from the MGM. Experiments were conducted to obtain this information and to estimate the value of C_{out} . These experiments consisted of measuring the volume of gas exiting the MGM during typical operation with a simple orifice flow meter, collecting samples of the gas, and analyzing these samples for CO₂ (carbon) content with a gas chromatograph.

3.2.2.1. ORIFICE FLOW METER

An orifice flow meter was employed to measure the gas venting rate from the MGM. Gas is regularly discharged from the MGM through a nominal 3 inch diameter PVC pipe connected to the headspace to prevent overpressurization due to the injections of air (for the airlift system) and CO₂ into the photobioreactor. Different types of flow meters were evaluated for this application and the orifice flow meter was determined to be durable and sufficiently accurate; it also provided a good compromise between cost and performance. The orifice flow meter was attached to the end of the 3 inch vent tube.

A photograph of the orifice meter and the connector piece used to attach it to the MGM vent is provided in Figure A.3 of Appendix A. The orifice flow meter consisted of a nominal 3 inch diameter PVC pipe and fittings upstream and downstream of the orifice plate. The ASME sharp edge orifice was machined from a Plexiglas plate and was sandwiched between the PVC pipe flanges. Several orifices were fabricated with different diameters to accommodate a range of possible flow rates. The orifice that was used in the tests had an internal diameter of 1.2 inches (3.0 cm). Pressure drop across the *vena contracta* taps was monitored with a Magnehelic differential pressure gauge. ASME relationships for sharp edge orifice response were then used to determine the flow rate from the measured pressure drop.

3.2.2.2. GAS SAMPLING AND ANALYSIS

The orifice flow meter was used to measure the gas venting rate. In order to determine C_{out} , the concentration of carbon in the gas being vented must be known. MGM gas samples were collected at the Mera Pharmaceuticals facility and brought to Honolulu for analysis.

Tygon tubing was inserted into the vent downstream of the orifice and samples were extracted with a vacuum pump and stored in 1 liter Teflon sampling bags. An inline filter removed water vapor from the vented gas. Figure A.4 in Appendix A shows the simple gas sampling system used in the experiments.

3.2.2.3. GAS VENTING EXPERIMENTS

Experiments were conducted to measure MGM vent flow rate and to collect vent gas samples at the Mera Pharmaceuticals facility in Kona. Figure A.5 in Appendix A presents a photograph of the orifice flow meter and gas sampling system installed at the end of the downward-facing MGM vent tube.

During the experiments, the automated CO₂ injection system was turned off so that the start time and duration of the CO₂ injections could be manually adjusted. Tests were performed where CO₂ was injected continuously into the MGM for 21 minute periods. The amount of pure CO₂ injected was monitored and recorded. Vent gas samples and differential pressure readings (*i.e.*, vent gas flow rates) were taken before, during, and after the injections.

The gas samples were brought back to University of Hawai‘i at Mānoa for gas chromatography analysis using a Shimadzu Model 14A gas chromatograph (GC). Figure A.4 in Appendix A presents a photograph of the Shimadzu Model 14A GC. The 0.2 mL samples were manually injected into the GC using a gastight syringe. The injected sample was carried through the column by an inert carrier gas consisting of 8% hydrogen and 92% helium by volume. The sample was partitioned between the carrier gas and a stationary phase supported on an inert size-graded solid (solid support) in a packed column. A Carbonex 1000 packed column was used for this analysis. The solvent selectively impeded the sample components, depending on their distribution coefficient, until they formed separate bands in the carrier gas (Clausen, 2004). These individual bands left the column in the gas stream and were recorded as a function of time by a detector.

The measurements were performed with a thermal conductivity detector (TCD) in which a tungsten filament is heated by a constant 100 mA electrical current. The TCD has the ability to conduct heat from a filament which is a function of the molecular weight of the gas. In these measurements, both the temperatures of the injection port and the detector were set at 140° C. The column temperature was programmed to start at 45° C, maintain that temperature for 1 minute, increase 20° C for each of the next seven minutes, maintain 185° C for 1 minute, and finally cool down for 11 minutes before the next run.

The GC was calibrated using three gas standards: pure N₂; 0.038% CO₂ in atmospheric air; and a mixture of 2.1% CO₂ in 97.9 % N₂. The same protocol was used during the calibration and the sample analysis with the exception that the gas standards were injected automatically into the GC.

The mass flow rate of carbon vented out of the MGM was calculated from the measured gas venting rate and the concentration of carbon in the gas samples. The total mass of carbon vented over the duration of the experiment was determined by integration of the experimental values of the mass flow rate of carbon. This value is divided by the total mass of carbon injected into the MGM during the duration of the experiment to estimate the percentage of injected carbon vented from the MGM. This percentage was used in the carbon mass balance and the process model.

3.2.3. Carbon Bound in Biomass

The daily rate of change in the concentration of carbon bound in the *Haematococcus pluvialis* biomass, $\frac{d[C_{biomass}]}{dt}$ cannot be determined directly from operational data provided by Mera Pharmaceuticals, Inc. but can be estimated by analysis of cell samples collected on a daily basis. $\frac{d[C_{biomass}]}{dt}$ was estimated by comparing the mass of carbon bound in the cells on consecutive days. The mass of carbon in the cell biomass pool is the product of the total cell count (or concentration) in the MGM, the average dry cell mass, and the average % total organic carbon (%TOC) of a cell on a dry mass basis. Mera Pharmaceuticals regularly monitors the quantity of cells in the MGM and this information is provided in the MGM operational data. Occasionally, Mera Pharmaceuticals collects cell samples to determine the dry cell mass, but does not monitor the %TOC in a cell.

Mera Pharmaceuticals, Inc. provided dried samples of *Haematococcus pluvialis* for %TOC analysis by the University of Hawai'i. These samples were collected from the MGM identified as M13A-030423 over a period of 6 days at different times during both the day and night cycles. Table 3.1 summarizes the information for this set of samples, including sampling dates and times, ages relative to the time of initial inoculation of the MGM, average cell count, liters of culture and media sampled, and dry masses. Using this information, the daily average dry cell mass and the average dry cell mass over the 6 days that samples were collected were calculated. The Agricultural Diagnostic Service Center of the University of Hawai'i analyzed the *Haematococcus pluvialis* samples for %TOC on a dry mass basis. The product of the %TOC results, the data on cell counts

(concentrations), and average dry cell mass was the daily mass of carbon bound in the biomass. The change in mass of carbon bound in the biomass between consecutive days could then be used to estimate $\frac{d[C_{biomass}]}{dt}$.

Table 3.1. *Haematococcus Pluvialis* Samples

Date	Time	Age (days)	Average Cell Count (cells/mL)	Liters used	Dry Mass (g)
4/26/03	5:40	3	156,513	3	0.3498
4/26/03	18:45	3	237,617	3	0.6309
4/27/03	5:40	4	211,803	3	0.4901
4/27/03	18:30	4	298,501	3	0.6839
4/28/03	6:05	5	304,173	3	0.6213
4/28/03	18:50	5	336,370	1.95	0.6501
4/29/03	5:30	6	410,071	3	0.9152
4/29/03	18:45	6	441,130	2	0.7105
4/30/03	6:00	7	431,003	2	0.7581
4/30/03	19:00	7	538,085	2	1.0871
5/1/03	5:25	8	520,702	2	0.9908

3.2.4. Change in Carbon Concentration in the Headspace

Determination of the final unknown term in the mass balance equation,

$\frac{d[C_{headspace}]}{dt}$, the daily rate of change in carbon concentration in the headspace posed a problem, since this requires a detailed time history of the headspace gas concentration, which is not monitored by Mera Pharmaceuticals. Resources were not available to conduct long term extractive sampling of the vent gas and subsequent GC sample analysis. Given that the efficiency of carbon capture by the biomass (which is essentially

the ratio of $V_l M_c \frac{d[C_{biomass}]}{dt}$ and C_{in}) was the primary interest of this study and that the carbon mass balance served as a check to verify the values of $\frac{d[C_{biomass}]}{dt}$ and C_{in} , it was decided to forego experiments needed to determine $\frac{d[C_{headspace}]}{dt}$. $\frac{d[C_{headspace}]}{dt}$ was instead determined from the carbon mass balance equation (since it is the only unknown) and its values were assessed on the assumption that CO_2 equilibrium existed between the liquid media and gas headspace. This assumption should be tested in future studies where long term data histories are collected simultaneously of gas headspace composition and media pH and alkalinity (to calculate DIC).

3.2.5. Relationships Between Variables in the Carbon Mass Balance Equation

After all terms in the carbon mass balance equation were calculated, relationships between different variables in this equation were developed and used in the process model. One relationship of interest was the variation in mass flow rate of carbon injected into MGM over time. The mass flow rate of carbon is controlled automatically in response to changes in media pH. Specifically, we were interested in whether carbon injections were random, constant, increasing, or decreasing. Relationships also were derived to determine if the quantity of carbon dissolved in the media or the quantity of carbon degassed out of the media is affected by a change in the quantity of carbon injected into the MGM; and if either the change in mass of carbon bound in the biomass

or the change in dissolved inorganic carbon concentration is affected by a change in the total carbon in the media.

3.3. *Haematococcus pluvialis* Population

Haematococcus pluvialis utilizes carbon from the CO₂ and air injections for cell production (division). The relationship between the cell division rate and the average rate of carbon uptake per cell was of interest in this study.

The specific growth rate (*i.e.*, the population-averaged rate of cell divisions per cell) is given by:

$$\mu = \frac{\ln \left[\frac{B_0 + Y}{B_0} \right]}{\delta t} \quad (3.7)$$

where B₀ is the initial number of cells in the culture and Y is the number of cells created over the time interval δt (Geider & Osborne, 1992). The average rate of carbon uptake per cell could be estimated by dividing the change in the total mass of carbon bound in the biomass between two consecutive days (see Section 3.2.3) by the *Haematococcus pluvialis* population on the first day of the two consecutive days. These data were analyzed and a relationship between carbon uptake and specific growth rate was developed.

3.4. Harvesting Strategy

The criteria for the harvesting strategy applied in the process model simulations were determined by reviewing Mera Pharmaceuticals' operating records. The records indicate that the current Mera Pharmaceuticals harvesting criteria are based on two parameters: (1) a specific number of cells needed to inoculate the open ponds and (2) a minimum cell concentration in the MGM that must be achieved before harvesting. Values of these two parameters were identified by examination of the MGM operational data.

3.5. STELLA Model

The process model was developed using the STELLA software. STELLA is a computer software program with an interface for building dynamic models that realistically simulate biological systems (Rice *et al.*, 2002). The procedure used in STELLA modeling involves: (1) constructing a relational model of the system using icons that represent state and rate variables and arrows and flows that represent interrelated components; (2) quantifying the relationships among elements in the model; and (3) running the model to observe the system dynamics (American Society for Horticultural Science, 2004; Rice *et al.*, 2002).

The process model integrates the partitioning of the carbon, *Haematococcus pluvialis* population dynamics, and the harvesting strategy. The carbon component of the model incorporated different variables of the carbon mass balance, Equation 3.2, such as the mass flow rates of carbon injected into and vented out of the MGM, and changes in

mass of dissolved inorganic carbon, carbon bound in the biomass, and carbon in the headspace. The relationships between variables in the carbon mass balance equation described in Section 3.2.5 were included in the model. The *Haematococcus pluvialis* population component of the model describes the growth rate of the cells and their ability to capture and assimilate CO₂ as a function of operating conditions.

3.6. Model Verification

The process model was verified by comparison of its results with operational data from a different MGM than the one used to develop the functional relationships between variables used by the model. Data from MGM identified as M10A-040810 were employed. Model inputs from the operational records of this MGM included the carbon injection mass flow rates, the initial cell population, media volume, target concentration (for harvesting), and the harvesting cell quantity. The simulated output was the cell population size. Statistical techniques were used to compare the simulated outputs and the data to determine whether the model provides an accurate representation of the photobioreactor (Law & McComas, 2001).

3.7. Sensitivity Analysis

After the model was verified, analyses were conducted to determine the sensitivity of the predicted amount of carbon captured to varying the target cell concentration and the harvesting cell quantity. One of these two input was varied at a

time, while other model parameters were held constant, to see the resulting impact on the model output.

3.8. Model Simulations

Different operating scenarios were simulated with the process model to identify the combination of the target cell concentration and the harvesting cell quantity that would yield maximum carbon capture. Maximizing carbon capture is the same as maximizing cumulative cell yield since the model assumes a constant %TOC per cell.

CHAPTER 4. RESULTS AND DISCUSSION

This Chapter presents the results of this study. The experimental results for determining the venting rate from the MGM and mass of carbon in the cell biomass pool are discussed first. The carbon mass balance calculations and the derivation of functional relationships used by the process model are presented next. Finally, the completed process model, results of the model verification and sensitivity analyses, and harvesting simulations are provided.

4.1. Carbon Venting Rates from the MGM

Table 4.1 summarizes the measured flow rates of gas vented from the MGM and the corresponding carbon concentrations in that gas determined following the procedures described in Chapter 3.

Table 4.1. Vent Flow Rate and Vented Carbon Concentration from MGM

Time	Vent Flow Rate (L/min)	Vented Carbon Concentration (g/L)
14:52	580.78	1.46E-03
15:00	554.08	2.41E-03
15:09	554.08	2.28E-03
15:14	580.78	2.39E-03
15:20	554.08	2.59E-03
15:25	580.78	1.34E-03
15:30	580.78	1.33E-03
15:35	580.78	1.47E-03
15:40	580.78	7.81E-04
15:45	580.78	7.77E-04

Gas flow rate varied between 554.08 L/min and 580.78 L/min and the vented carbon concentration ranged from 7.77×10^{-4} g/L to 2.59×10^{-3} g/L over the 53 minute duration of the experiment. The vent flow rate was observed to be relatively steady; the difference in the two values in the Table corresponds to the smallest change in pressure drop that could be resolved with the Magnehelic differential pressure gauge. The mass flow rate of carbon vented out of the MGM was calculated from data in Table 4.1 and is presented in Table 4.2.

Table 4.2. Mass Flow Rate of Vented Carbon from MGM

Time	Mass Flow Rate of Vented Carbon (g/min)
14:52	0.845
15:00	1.336
15:09	1.266
15:14	1.390
15:20	1.434
15:25	0.776
15:30	0.770
15:35	0.856
15:40	0.454
15:45	0.452

The mass flow rate of carbon vented out of the MGM increased from 0.845 g/min at 14:52 to 1.434 g/min at 15:20 and then decreased to 0.452 g/min at 15:45. CO₂ was injected into the MGM media at a constant rate of 11.80 L/min between 14:54 and 15:05. This sparging resulted in an increase in the mass flow rate of vented carbon that persisted for about 20 minutes after the CO₂ injection was terminated.

The discrete carbon flow rate data were integrated numerically using Matlab to determine the total mass of carbon vented from the MGM over the entire duration of the experiment. This quantity was divided by the total mass of carbon entering the MGM via the CO₂ and air injections over the duration of the experiment to estimate the percentage of carbon vented. The carbon loss during the experiment was 41.4%. This value was used in the carbon mass balance equation to represent the fraction of CO₂ entering the MGM during the day that is eventually vented. It was also assumed that all the carbon contained in the air injections is vented during the night, when photosynthesis ceases and there is no CO₂ sparging into the liquid media. There may be additional loss of carbon from the MGM, which currently is not accounted for, since CO₂ outgassing from the media may occur at night and this carbon will be vented along with the CO₂ in the air injections. Additional experiments must be conducted to determine accurately the value of the carbon loss.

4.2. Carbon Assimilated by Biomass

Average dry cell mass, average %TOC on a dry mass basis, and the number of cells in the MGM were used to calculate the daily mass of carbon bound in the biomass. Average dry cell mass determined from the data in Table 3.1 and the results of the %TOC analysis of these samples are presented in Table 4.3.

Table 4.3. Dry Cell Mass and %TOC for *Haematococcus pluvialis* Samples

Date	Time	Dry Cell Mass (g)	Total Organic Carbon (%)
4/26/03	5:40	7.45E-10	40.03
4/26/03	18:45	8.85E-10	41.41
4/27/03	5:40	7.71E-10	42.17
4/27/03	18:30	7.64E-10	42.70
4/28/03	6:05	6.81E-10	43.18
4/28/03	18:50	9.91E-10	42.82
4/29/03	5:30	7.44E-10	43.15
4/29/03	18:45	8.05E-10	43.79
4/30/03	6:00	8.79E-10	43.74
4/30/03	19:00	1.01E-09	45.23
5/1/03	5:25	9.51E-10	46.01

Table 4.3 indicates that the dry cell mass varied between 6.81×10^{-10} g and 1.01×10^{-9} g over the 6 days of sampling and %TOC ranged from 40.03% and 46.01% over this period. The average and standard deviation of the morning values for the dry cell masses were 7.95×10^{-10} g and 1.00×10^{-10} g, respectively. The average absolute error of the morning values for the dry cell masses was 1.29×10^{-13} g. The average and standard deviation of the morning values of %TOC were 43.05% and 1.96%, respectively. This value is reasonable compared to data in the literature that report typical dry mass %TOC of microalgae of approximately 50% (Becker, 1994).

The dry cell mass and %TOC were employed to estimate the mass of carbon per cell. The mass of carbon per cell over the six day period is plotted in Figure 4.1. The mass of carbon per cell is observed to vary between 2.98×10^{-10} g and 4.57×10^{-10} g, generally increasing during the day via photosynthesis and decreasing at night due to respiration. There appears to be an increasing trend over time.

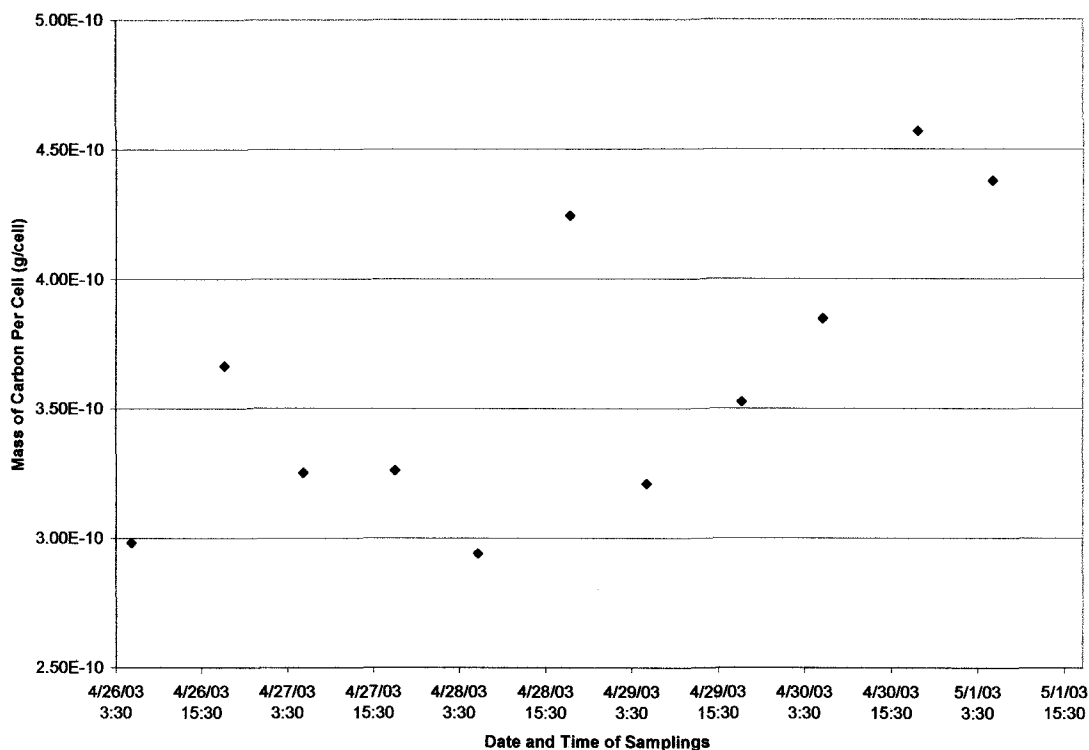


Figure 4.1. Mass of carbon per cell.

4.3. Carbon Mass Balance Calculations

Using the results of the gas venting experiments, cell sample analysis, and the MGM operational data, values of the different terms in the carbon mass balance equation (Equation 3.1) were calculated and are shown in Table 4.4. The data were from MGM identified as M13A-020423 which operated from April 23, 2003 to May 27, 2003. It should be noted that entries in Table 4.4 are not continuous; results are missing for a number of dates since the daily data set provided by Mera Pharmaceuticals was incomplete. Data were not provided for the period around the harvesting dates of May 1, 2003, May 6, 2003, May 9, 2003, May 14, 2003, May 19, 2003, May 23, 2003, and May 27, 2003. When the MGM is harvested, a portion of the liquid media (about 50%) and

the cells contained therein is extracted and transferred to the open ponds. Fresh media is then added to the MGM to compensate for the amount removed.

Table 4.4. Carbon Mass Balance for MGM

Date	Carbon Injected into MGM (g/day)	Carbon Vented Out of MGM (g/day)	DIC (g/day)	Carbon Bound in Biomass (g/day)	Carbon in Gas Space (g/day)
4/26/03	899.61	443.56	70.89	218.86	166.30
4/27/03	898.34	441.25	58.34	341.92	56.83
4/28/03	1051.91	499.30	65.77	408.74	78.10
4/29/03	1011.39	478.98	51.21	69.64	411.56
5/3/03	962.70	465.43	12.80	210.90	273.57
5/4/03	1107.51	520.48	189.21	381.25	16.56
5/7/03	1628.55	686.29	115.98	540.11	286.16
5/8/03	1691.50	742.69	169.60	349.94	429.28
5/10/03	1488.99	668.02	94.87	480.92	245.18
5/11/03	1526.21	673.93	112.90	381.29	358.08
5/12/03	1684.59	745.34	71.50	256.54	611.20
5/13/03	1784.24	782.69	44.97	326.89	629.69
5/15/03	1376.35	628.38	72.97	415.10	259.90
5/16/03	1588.86	706.96	134.41	614.64	132.84
5/17/03	1715.64	750.62	29.03	381.69	554.31
5/18/03	1914.07	816.54	125.51	282.84	689.17
5/21/03	1558.77	691.16	92.91	375.37	399.32
5/22/03	1785.67	782.66	135.44	393.48	474.09
5/25/03	1914.77	832.19	68.11	676.68	337.78
5/26/03	1770.71	776.55	124.56	257.20	612.40

Table 4.4 indicates that the daily mass flow rates of carbon injected into and vented out of the MGM varied between 898.34 g/day and 1914.77 g/day and between 441.25 g/day and 832.19 g/day, respectively. The respective ranges of the changes in dissolved inorganic carbon, carbon bound in biomass, and carbon in the headspace were 12.80 g/day to 189.21 g/day, 69.64 g/day to 676.68 g/day, and 16.56 g/day to 689.17 g/day.

The percentage of injected carbon that is assimilated into the biomass pool (*i.e.*, the ratio of carbon bound in biomass divided by the carbon injected into the MGM)

ranged from around 7% to 39% with a cumulative average of 25%. This suggests that additional research needs to be conducted to improve the carbon capture efficiency. One possibility may be a system where vented gases are recirculated back into the photobioreactor. The effect of recirculation on microalgae growth and other technical and economic factors will need to be investigated.

The results provide insight into the behavior of the MGM system. Since the daily rate of change of carbon bound in cell biomass ($\frac{d[C_{biomass}]}{dt}$) is observed generally to be significantly greater than the increase in the DIC pool in the media ($\frac{d[DIC]}{dt}$), it appears that CO₂ that is injected and dissolves into the liquid is being effectively assimilated by the cells.

The results in Table 4.4 indicate that carbon accumulates continuously in the liquid media (as DIC) and the headspace. The accumulation of DIC in the media is determined directly from data on pH and alkalinity. The accumulation of CO₂ in the headspace, however, is an inferred quantity and strongly reflects the measured daytime carbon venting rate, which is taken to be a fixed percentage of the CO₂ injection rate. At night, it is assumed that the carbon venting rate falls to exactly equal the rate on carbon entering the MGM with the airlift injections. It is possible that CO₂ venting losses exceed the amount of CO₂ entering the MGM during the night, reducing or negating the calculated accumulation in the headspace. Under this scenario, CO₂ concentrations in the headspace may fall to levels comparable to the CO₂ concentration in air during the night. Assuming that all of the CO₂ advected into the MGM with the airlift injections, the

equation for the nighttime concentration of CO₂ in the headspace, y , as a function of time is:

$$y = y_{atm} \left[1 - e^{-\left(\frac{Q}{V_g} t\right)} \right] + y_0 e^{-\left(\frac{Q}{V_g} t\right)} - \left(\frac{V_l}{V_g}\right) [DIC]_t + \left(\frac{V_l}{V_g}\right) [DIC]_0 e^{-\left(\frac{Q}{V_g} t\right)} + \left(\frac{V_l Q}{V_g^2}\right) e^{-\left(\frac{Q}{V_g} t\right)} \int_0^t [DIC]_{\tau} e^{-\left(\frac{Q}{V_g} \tau\right)} d\tau \quad (4.1)$$

where y_{atm} is the carbon dioxide concentration in air (mol/L), Q is the volumetric air flow rate into the MGM (L/min), V_g is the volume of the headspace (L), t is the time (min), y_0 is the initial headspace CO₂ concentration (mol/L), V_l is the volume of the media (L), $[DIC]_t$ is the dissolved inorganic carbon concentration at time t (mol/L), $[DIC]_0$ is the initial dissolved inorganic carbon concentration (mol/L), and τ is the variable of integration.

Nighttime alkalinity data needed to determine $[DIC]$ was only available for the first few days that the MGM was operational; hence, overnight headspace CO₂ concentration as a function of time was calculated using Equation 4.1 for April 26, 2003 and April 27, 2003. These results are plotted in Figures 4.2 and 4.3, respectively.

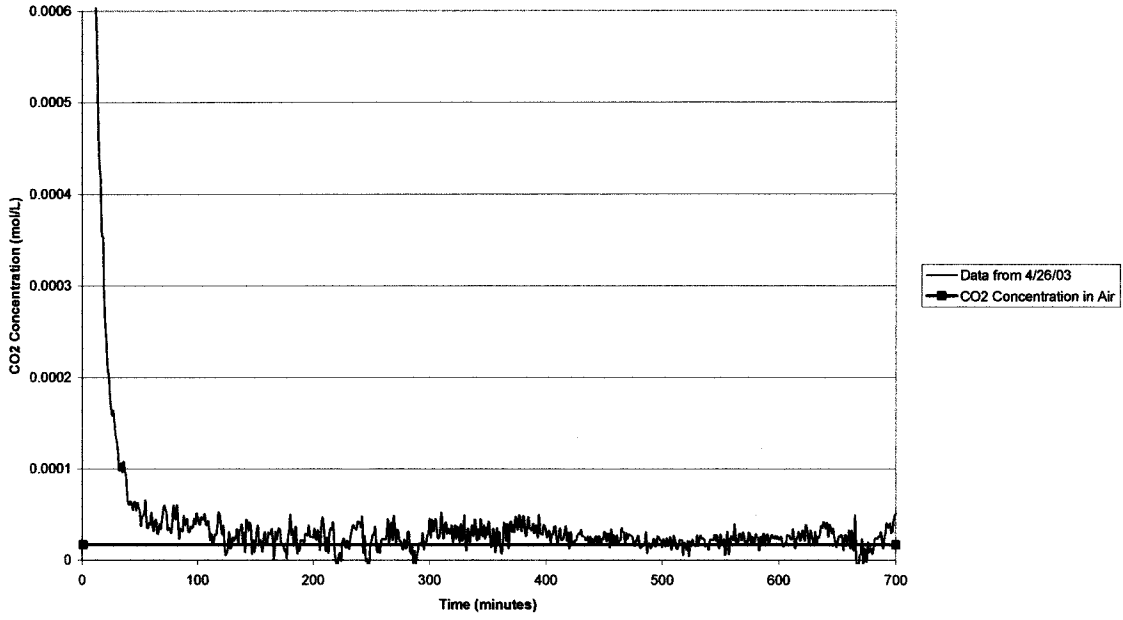


Figure 4.2. Nighttime headspace CO₂ concentration for 4/26/03.

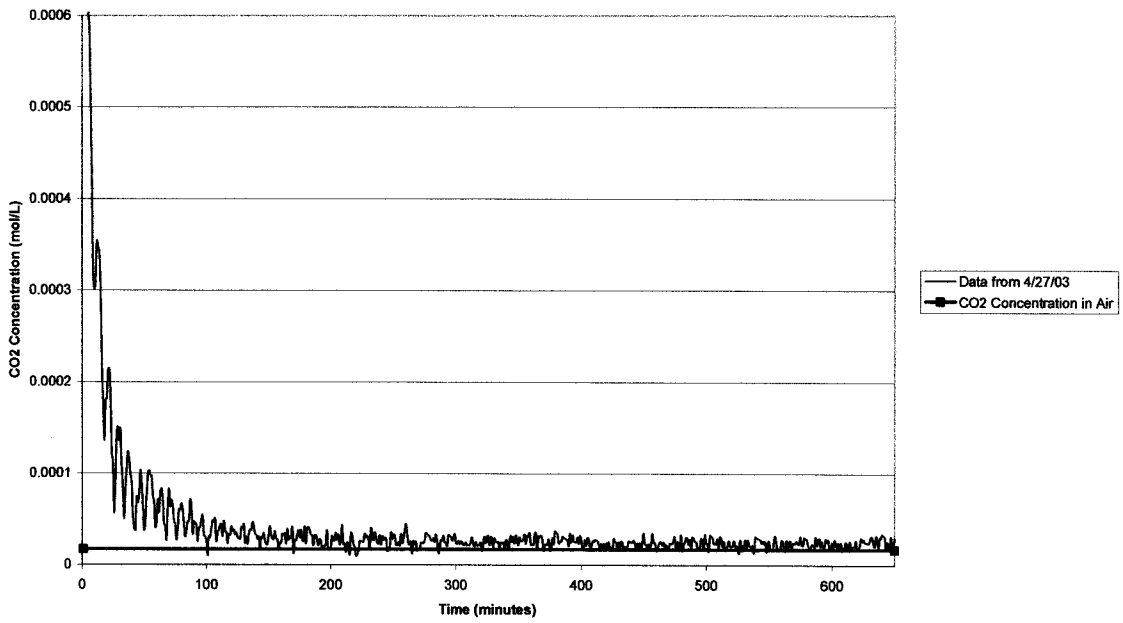


Figure 4.3. Nighttime headspace CO₂ concentration for 4/27/03.

Figures 4.2 and 4.3 indicate that CO₂ accumulated in the headspace during the day dissipates quickly to a level comparable to the concentration of CO₂ in air at night

which was 1.70×10^{-5} mol/L. It is reasonable to conclude, therefore, that the net daily change in carbon in the headspace was zero because accumulated CO_2 is vented out of the MGM at night. The daily amounts of carbon vented from the MGM should then equal the sum of the values given in columns 3 and 6 of Table 4.4.

4.4. Process Model Relationships

Relationships between different variables that appear in the carbon mass balance equation were derived and incorporated into the STELLA process model. The first relationship was for the daily mass flow rate of carbon injected into the MGM. The data and curvefit are plotted in Figure 4.4. The corresponding R^2 value of the linear curvefit is also included in the figure. Given the scatter in the data, a linear equation appears reasonable. The carbon injection rate responds to increasing pH due to carbon depletion in the media either by degassing of the carbon or photosynthetic utilization. Increasing carbon injection rates therefore indicate rising rates of depletion of carbon in the media.

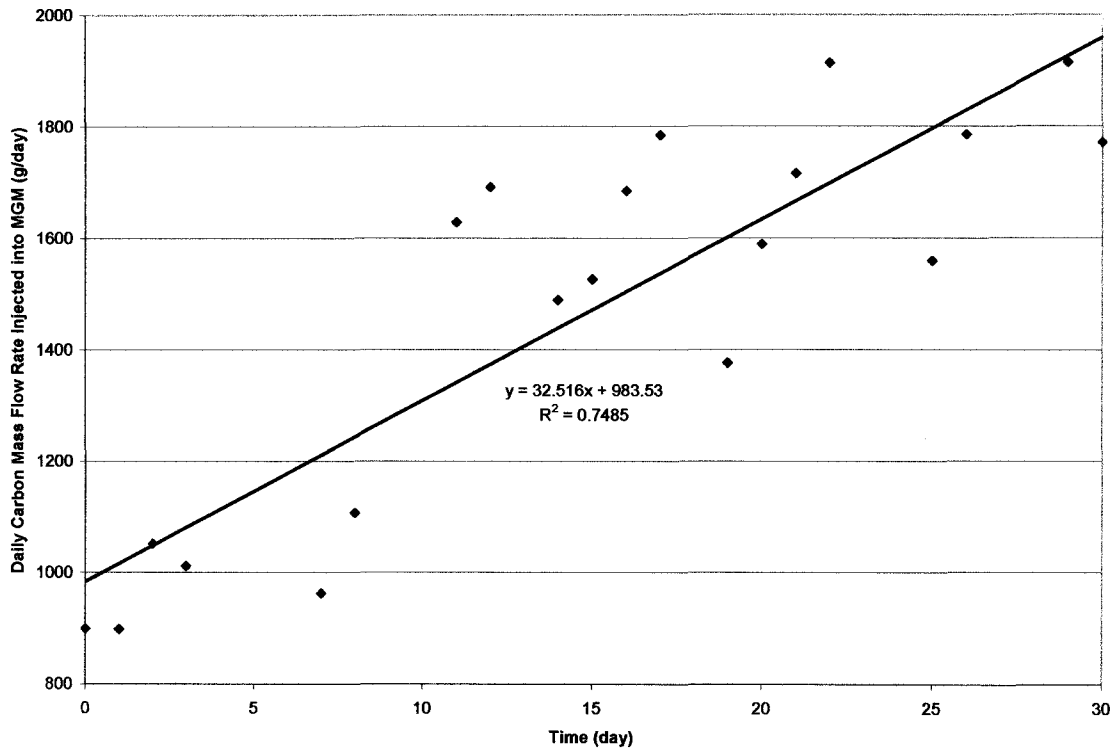


Figure 4.4. Daily carbon mass flow rate injected into the MGM over time.

Figure 4.5 plots the mass flow rate of carbon degassed from the media as a function of the daily rate of carbon injection into the MGM. The carbon degassing rate is the amount of injected carbon that does not dissolve in the media over the course of a day and is the sum of the daily carbon venting rate from the MGM and the change in carbon concentration in the headspace (columns 3 and 6 in Table 4.4). A linear curvefit to the data and the corresponding R^2 value are shown in the figure. Using this relationship, the partitioning of the injected carbon between the media phase, where the carbon is available for cell growth, and the gas phase, where carbon will eventually be vented, can be determined.

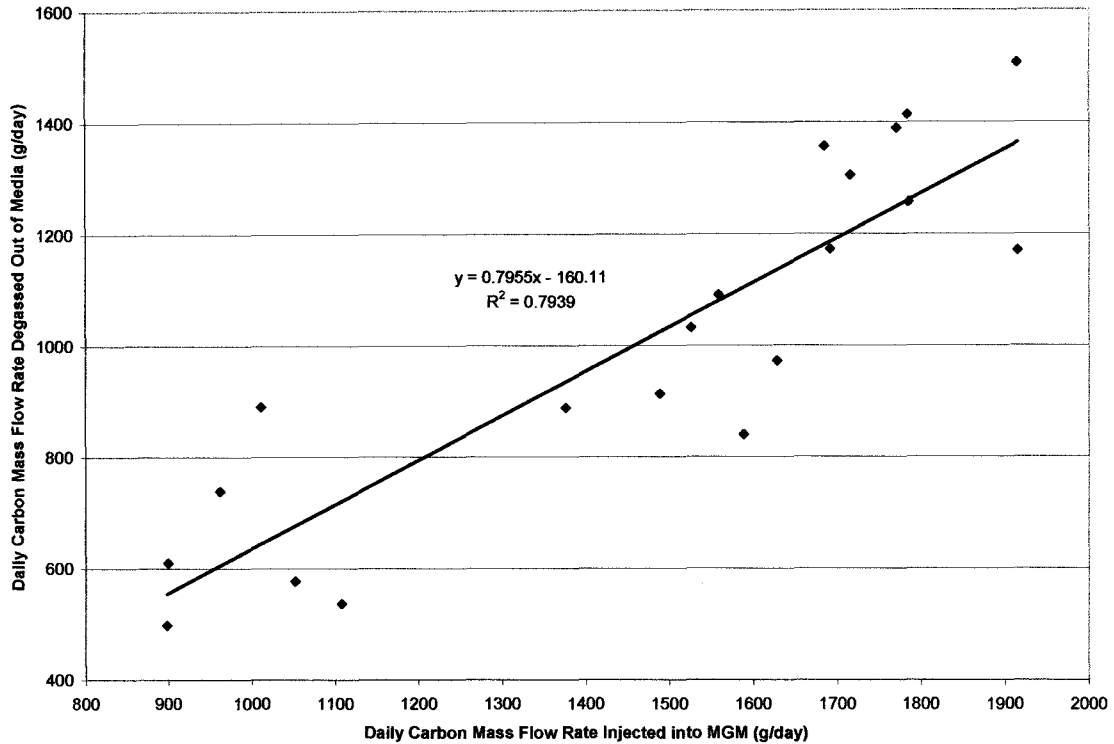


Figure 4.5. Daily carbon mass flow rate degassed out of the media vs. daily carbon mass flow rate injected into the MGM.

Figure 4.6 presents data on the daily change in the mass of carbon bound in biomass as a function of the daily change in the mass of total carbon in the media. The total carbon in the media is the sum of carbon bound in biomass and in the DIC pool. Again, the data suggest a linear relationship between these two quantities and a curvefit and corresponding value of R^2 are included in the figure. Using this relationship, the daily change in carbon bound in biomass can be estimated from the daily change in total carbon in the media, which is the difference between the daily carbon injection rate and the daily degassing rate. Note that the daily degassing rate can be determined by the equation given in Figure 4.5 from the carbon injection rate.

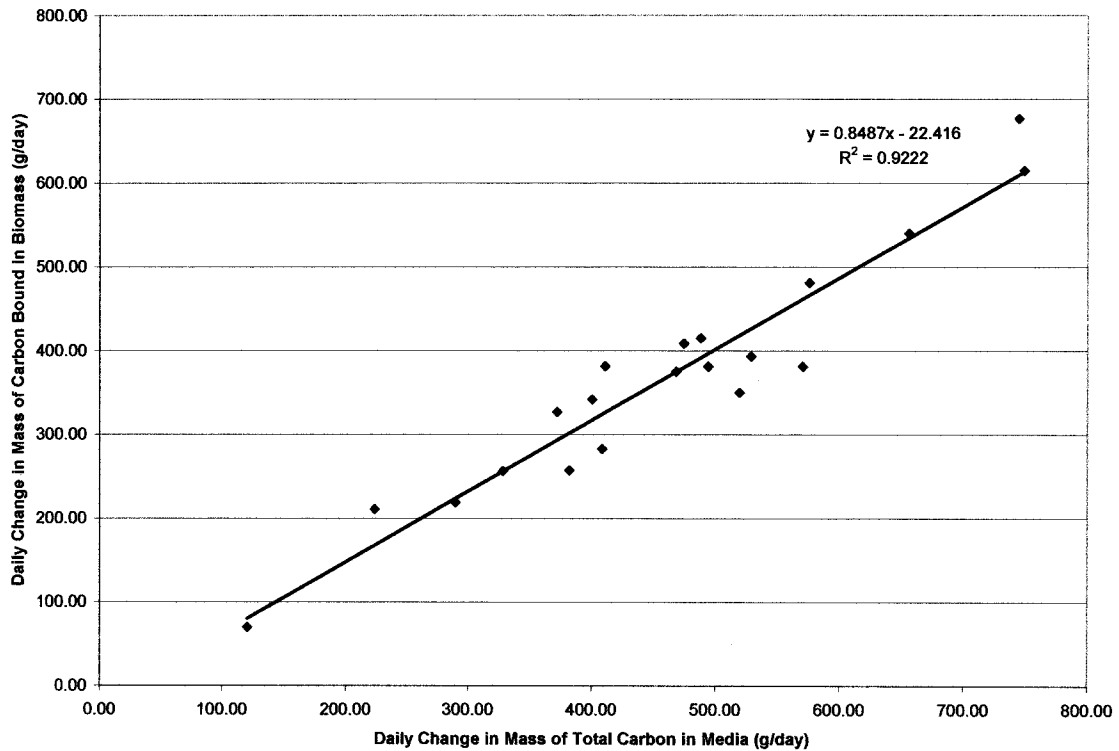


Figure 4.6. Daily change in the mass of carbon bound in biomass vs. daily change in the mass of total carbon in the media.

Finally, a relationship was derived for the daily specific growth rate as a function of the daily rate of carbon assimilation into the cell biomass pool. The daily specific growth rate is the number of cell divisions that occur per cell per day. The relationship quantifies how the rate of carbon assimilation by cells affects cell division. Data plotted in Figure 4.7 indicates that rate of cell division increases linearly with the amount of carbon captured by the biomass pool. The best fit curve and the corresponding R^2 value are included in the figure. The curvefit provides a means to estimate the increase in the cell population in the MGM given the amount of carbon bound in the biomass in a day.

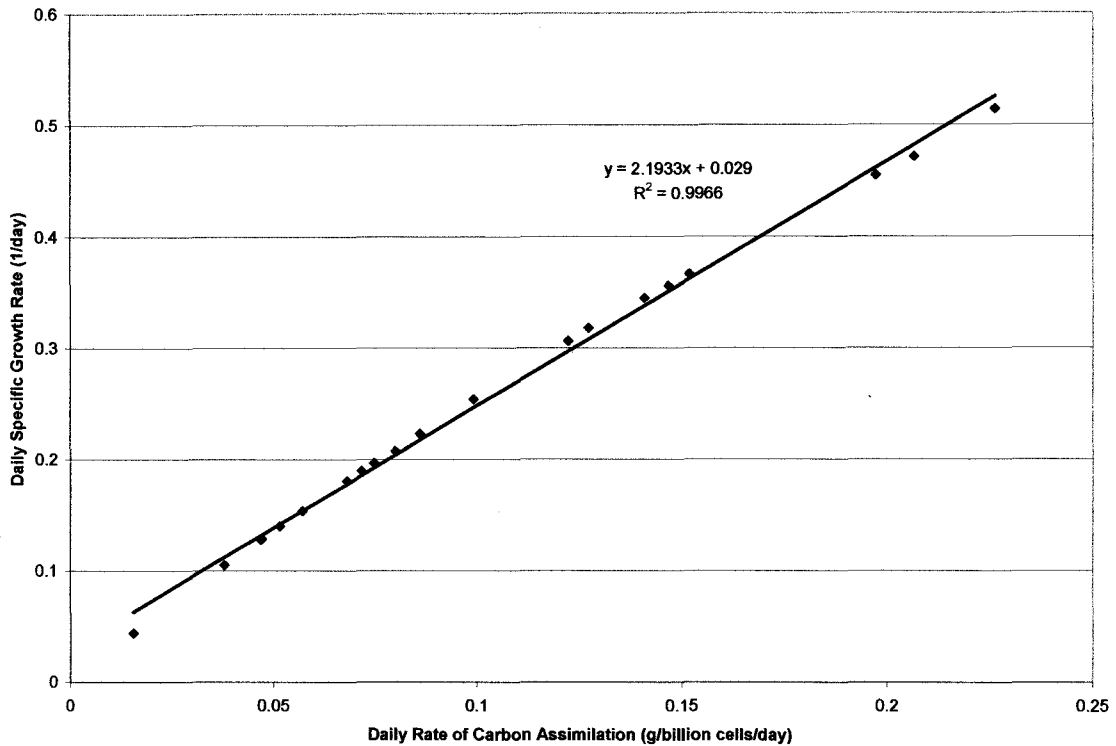


Figure 4.7. Daily specific growth rate vs. daily rate of carbon assimilation.

Taken together, the above relationships can be used to calculate the number of cells in the MGM at any time and the fate of injected carbon (dissolved, degassed, or bound in biomass) given the initial cell population and carbon injection rates (within the range of conditions of the data used to derive the relationships).

4.5. STELLA Process Model

A schematic drawing that summarizes the primary features of the *Haematococcus pluvialis* production process model that utilizes the STELLA software is shown in Figure B.1 in Appendix B. This model integrates the carbon mass balance, *Haematococcus*

pluvialis population dynamics, and the harvesting strategy using the relationships that were developed and the MGM operational data.

4.6. Verification of the STELLA Model

The STELLA process model was verified by comparison with data from MGM M10A-040810 following the procedure described in Section 3.6. Table 4.5 compares simulated population size and the data for M10A-040810. The results in Table 4.5 are plotted in Figure 4.8. The corresponding estimated percent errors of the simulations are given in Table 4.6.

Table 4.5. Comparison of Model Results and Data for MGM M10-040810

Date	Simulated Population Size (cells)	Population Size from Data Set (cells)
8/29/04	4.86E+12	5.44E+12
8/30/04	5.70E+12	4.23E+12
8/31/04	4.58E+12	5.12E+12
9/1/04	3.47E+12	3.9E+12
9/2/04	4.49E+12	4.75E+12

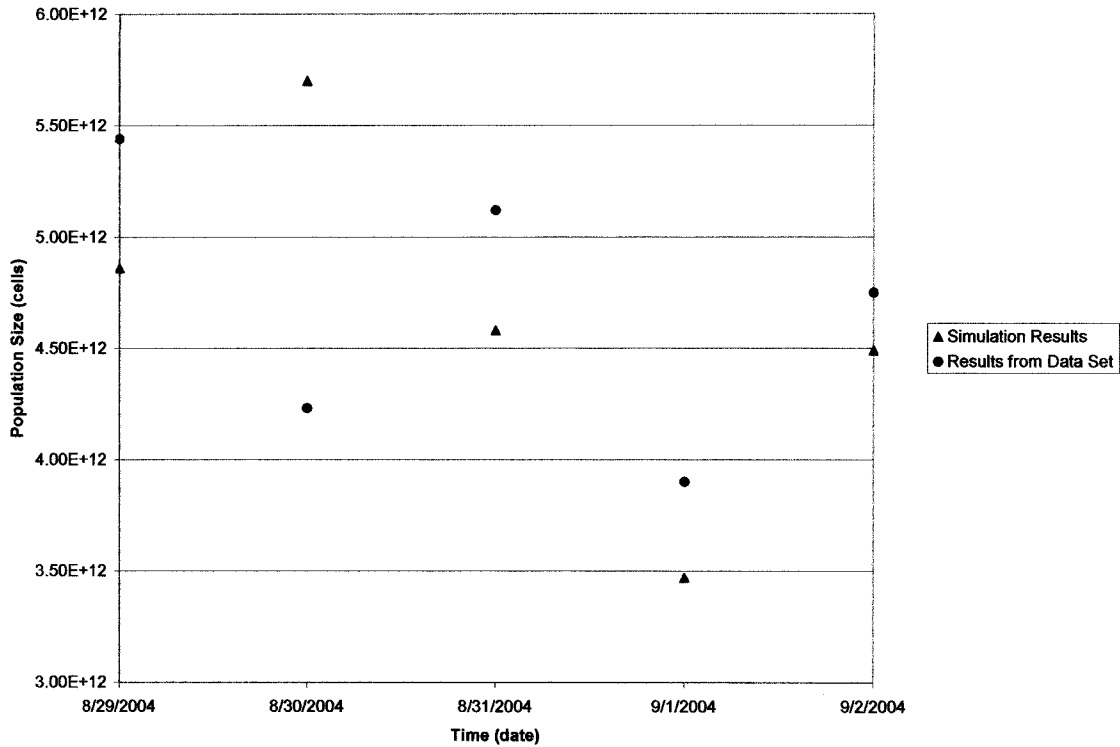


Figure 4.8. Comparison of model results and data for MGM M10-040810.

Table 4.6. Percent Error of Model Predictions of Cell Population for M10-040810

Date	Percent Error (%)
8/29/04	10.57
8/30/04	34.85
8/31/04	10.60
9/1/04	11.12
9/2/04	5.44

The percent error ranged from 5.44 % to 34.85% with no clear trend with regard to underpredictions and overpredictions. The average percent error for all five dates tested was 14.51%. This value appears to be biased by the single large error for 8/30/04. The model appears to simulate the MGM operation reasonably well, but additional data sets should be tested to confirm this finding.

4.7. Sensitivity Analysis

In the present investigation, harvesting strategy is based on two parameters: target cell concentration that must be achieved in the MGM before harvesting can take place and the number of cells collected during a harvest. Optimizing the harvesting strategy involves varying these two parameters to achieve a maximum cumulative cell yield (*i.e.*, sum of cells collected over all harvests for a given duration of MGM operation). Sensitivity analyses were conducted using the STELLA software to facilitate the optimization and also to gain insight into the predicted behavior of the *Haematococcus pluvialis* production process.

Mera Pharmaceuticals currently uses a target cell concentration at 521,000 cells/mL and harvesting quantity at 3.2 trillion cells. For the sensitivity analysis, target cell concentration was first varied from 300,000 cells/mL to 700,000 cells/mL in increments of 200,000 cells/mL while harvesting quantity was held fixed at 3.2 trillion cells. Harvesting quantity was next varied from 1 trillion cells to 5 trillion cells in increments of 2 trillion cells with target cell concentration fixed at 521,000 cells/mL. Results obtained using the sensitivity analysis function of STELLA are presented in Tables 4.7 and 4.8.

Table 4.7. Target Cell Concentration and Cumulative Yield from the Sensitivity Analyses

Target Cell Concentration (cells/mL)	Cumulative Yield (in billions of cells)
300,000	29,849
500,000	31,623
700,000	33,220

Table 4.8. Harvesting Quantity and Cumulative Yield from the Sensitivity Analyses

Harvesting Quantity (in billions of cells)	Cumulative Yield (in billions of cells)
1,000	31,623
3,000	30,813
5,000	30,031

Table 4.7 indicates that cumulative yield increases with target cell concentration. The cumulative yield grew by about 3.4 trillion cells as target cell concentration increased from 300,000 cells/mL to 700,000 cells/mL.

Table 4.8 indicates that cumulative yield decreases with increasing harvesting quantity. The cumulative yield decreased by about 1.6 trillion cells as harvesting quantity increased from 1 trillion cells to 5 trillion cells.

These results provide guidance on how best to optimize harvesting strategy. It appears that maximum cumulative yield may be approached by increasing the target cell concentration and decreasing the harvesting quantity.

4.8. Model Simulations

The STELLA process model was used to investigate different harvesting scenarios. In each of these scenarios, initial cell count, carbon injection rates, and the total number of days until the final harvest were the same. Only the harvesting criteria were different. Table 4.9 provides the target cell concentration in the MGM (which must be attained before each harvesting), the harvesting cell quantity, and the corresponding cumulative cell yield for six scenarios.

Table 4.9. Target Cell Concentration, Harvest Quantity, and Maximum Cumulative Yield for Six Scenarios

Scenario	Target Cell Concentration (cell/mL)	Harvested Quantity (in billions of cells)	Cumulative Yield (in billions of cells)
1	521,000	3200	30,943
2	300,000	1000	29,849
3	400,000	1000	30,756
4	500,000	1000	31,623
5	600,000	1000	32,436
6	700,000	1000	33,220

Table 4.9 indicates that cumulative yield increases as the target cell concentration was increased while holding harvesting quantity constant at 1×10^{12} cells. This result primarily reflects the larger number of cells in the MGM at the time of the final harvest, which is included in the cumulative yield. The maximum cumulative yield of 3.32×10^{13} cells occurs in scenario 6 that had the highest target cell concentration and the lowest harvesting quantity among the different scenarios tested, which is consistent with the results from the sensitivity analyses. While this yield exceeds the yield for the current harvesting strategy, scenario 1, by over 3×10^{12} cells, it may be unrealistic. Scenario 1 requires nine harvests spaced apart by several days to allow the concentration in the MGM to recover, while scenario 6 requires 27 daily harvests. Daily harvesting of the MGM would place a strain on the small labor force employed at the Mera Pharmaceuticals facility. Moreover, seven ponds are required to stress the *Haematococcus pluvialis* harvested from the MGM without wasting any microalgal cells under scenario 6, while only five ponds are currently available at the Mera Pharmaceuticals facility.

A realistic harvesting scenario that provided a cumulative yield greater than the yield obtained with the current harvesting strategy was determined by additional model simulations. Scenarios were investigated with harvesting quantity held constant at the current value of 3.2×10^{12} cells and target cell concentration varied between 5×10^5 cells/mL and 5.5×10^5 cells/mL. A target cell concentration of 5.5×10^5 cells/mL was found to produce the maximum cumulative yield of 3.12×10^{13} cells, a relatively insignificant increase of 2.57×10^{11} cells (approximately 0.7%) over the yield for the current harvesting strategy. It appears, therefore, that the current harvesting strategy may represent the best possible scenario when real constraints imposed by the limited labor force and number of available open ponds are taken into consideration. Nonetheless, the present results suggest that the process model can be a valuable tool to optimize carbon capture and revenue streams when planning new facilities.

CHAPTER 5. SUMMARY AND CONCLUSIONS

A process model of a commercial scale hybrid photobioreactor/open pond microalgae production system was developed to optimize harvesting strategy to maximize carbon capture (*i.e.*, cumulative yield). As part of this development, the carbon balance over the photobioreactor was investigated and relationships were derived for the partitioning of carbon between the different carbon pools including DIC in the liquid media, organic carbon in the cell biomass, and losses to the headspace and by venting. The relationship between carbon assimilation and cell division was also determined.

The data suggest that the carbon capture efficiency of the present photobioreactor system is modest. Between 7% and 39%, with a cumulative average of 25%, of the carbon sparged into the media is eventually assimilated into the cell biomass. Most of the remaining carbon is lost via degassing and venting. To maximize carbon capture efficiency, a closed system in which vented gas is recirculated back into the photobioreactor should be explored.

Process model verification tests indicate that cell population growth is predicted reasonably well; however, additional comparisons with operational data should be performed.

Simulations were conducted to identify harvesting scenarios that would maximize cell biomass yield (and, hence, carbon capture). It was determined that reducing harvesting quantities while increasing target cell concentrations in the photobioreactor could provide significant increases in cumulative yield (about 10%) compared to the harvesting strategy currently applied by Mera Pharmaceuticals, Inc. Unfortunately, this

would require daily harvests and additional ponds. A target cell concentration of 5.5×10^5 cells/mL and a harvesting cell quantity of 3.2×10^{12} cells produced a realistic (*i.e.*, achievable with the current labor force and ponds) cumulative yield of 3.12×10^{13} cells; however, this is only 2.57×10^{11} cells greater than the cumulative yield of the current harvesting strategy. The current harvesting strategy appears to represent the best possible scenario when real constraints imposed by the limited labor force and number of available open ponds are taken into consideration. Nevertheless, the present results suggest that a process model can be a valuable tool to optimize carbon capture and revenue streams when planning new facilities.

Since optimizing a harvesting strategy for large-scale production of microalgae is a new concept in microalgal modeling, further research in this area is warranted. One area of potential interest is to incorporate microalgal models that predict culture growth rate as a function of light intensity, light/dark cycle effects induced by cell position in the depth of the culture, average solar irradiance, or non-limiting nutrients into the model for optimizing a harvesting strategy (Csögör *et al.*, 1999; Molina Grima *et al.*, 1996; Pruvost *et al.*, 2002; Zonneveld, 1996).

APPENDIX A. PHOTOGRAPHS



Figure A.1. Photograph showing the front view of a MGM photobioreactor.



Figure A.2. Photograph showing the side view of a MGM photobioreactor.

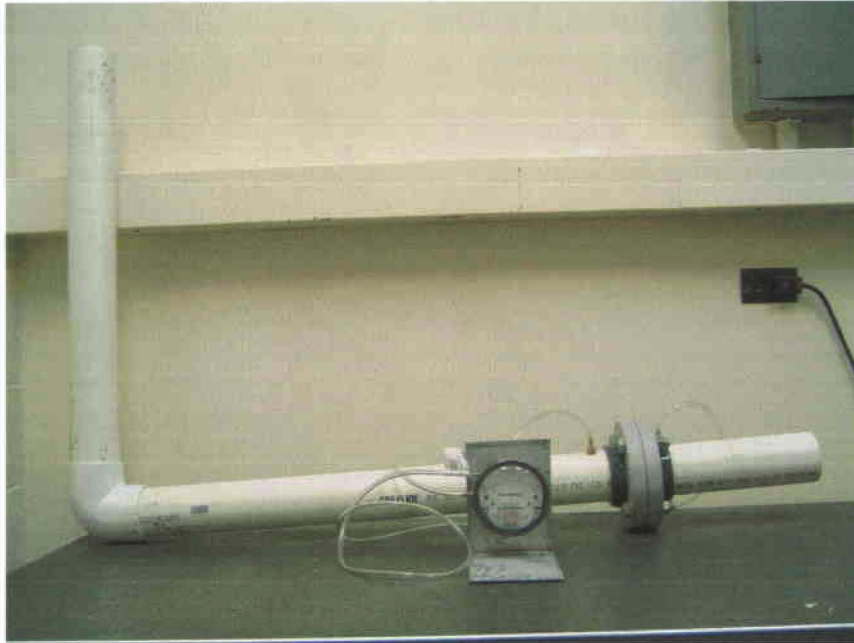


Figure A.3. Photograph showing the orifice meter and the connector piece.



Figure A.4. Photograph of the gas sampling system.



Figure A.5. Photograph showing the gas sampling system and the orifice meter attached to the photobioreactor vent at Mera Pharmaceuticals' facility.



Figure A.6. Photograph of the Shimadzu Model 14A gas chromatography.

APPENDIX B. STELLA MODEL

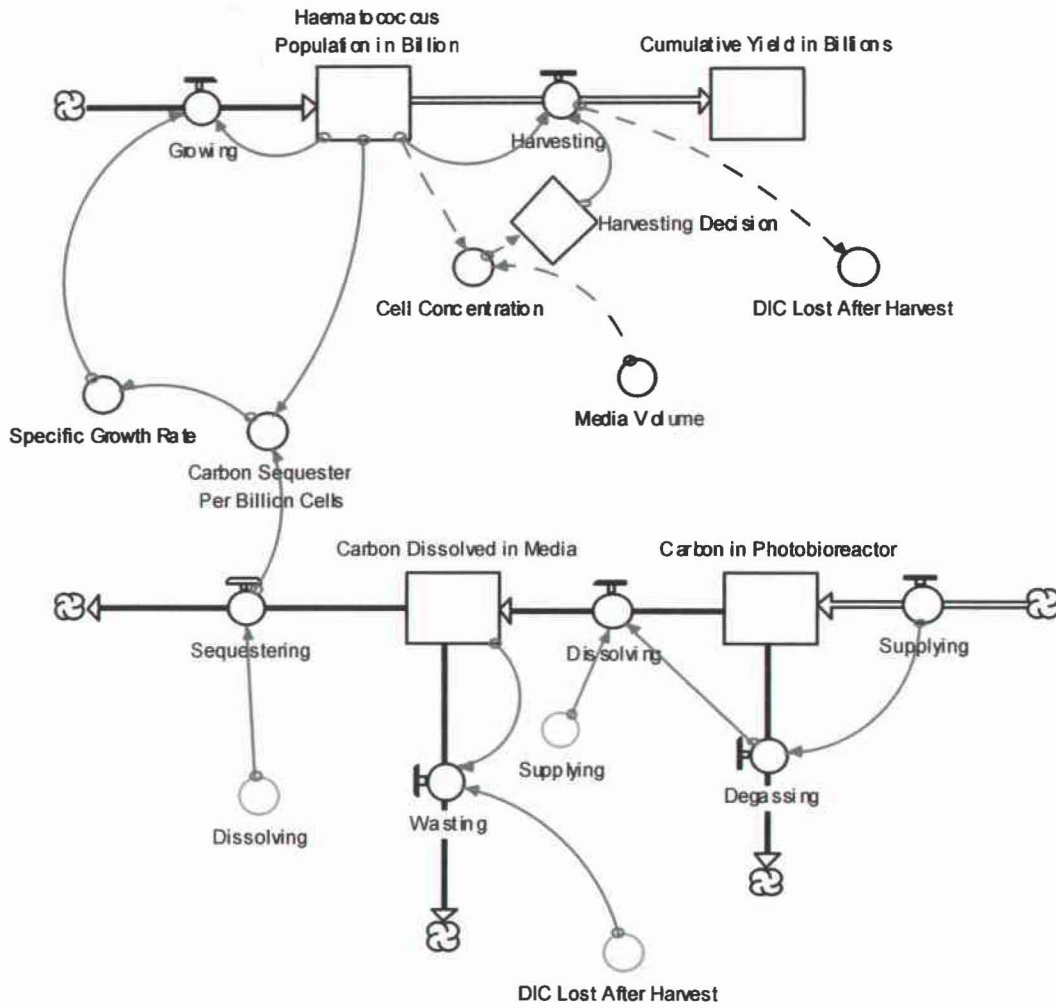


Figure B.1. Completed STELLA model.

REFERENCES

American Society for Horticultural Science (2004) Kent Kobayashi: using computer simulation software to enhance student learning. <http://www.ashs.org/resources/horteducator/Kobayashi.html>. 12 September 2004.

Becker, E.W. (1994) *Microalgae: Biotechnology and Microbiology*. Cambridge University Press, Cambridge, New York, pp. 1-2 and 11-13.

Beta Immune (2004) Astaxanthin – frequently asked questions. <http://www.beta-glucan-info.com/astaxanthin-questions-answers.htm>. 11 September 2004.

Buchdahl, J., Twigg, R., and Cresswell, L. (2002) Global warming: fact sheet series for key stages 2 & 3. http://www.ace.mmu.ac.uk/Resources/Fact_Sheets/Key_Stage_3/Global_Warming/pdf/Global_Warming.pdf. 22 September 2004.

Clausen, E.C. (2004) Lab I – experiment manual – gas chromatography. <http://ua-cheme.engr.uark.edu/classes/coursematerials/1212/web/11gc.htm>. 30 September 2004.

Csögör, Z., Herrenbauer, M., Perner, I., Schmidt, K., and Posten, C. (1999) Design of a photo-bioreactor for modeling purposes. *Chemical Engineering Processing* 38(4-6): 517-523.

Dugan, G.L. (1980) *Algal mass culture: principles, procedures, and prospects*. HNEI 81-02. Hawai'i Natural Energy Institute, Honolulu, Hawai'i, pp. 1-2 and 4.

Fábregas, J., Otero, A., Maseda, A., and Domínguez, A. (2001) Two-stage cultures for the production of astaxanthin from *Haematococcus pluvialis*. *Journal of Biotechnology* 89(1): 65-71.

Geider, R.J. and Osborne, B.A. (1992) *Algal Photosynthesis: the Measurement of Algal Gas Exchange*. *Current Phycology* 2. Chapman and Hall, New York, pp. 24-25.

Guerin, M., Huntley, M., and Olaizola, M. (2002) *Haematococcus* astaxanthin: health and nutritional applications. 1st Congress of the International Society for Applied Phycology/9th International Conference on Applied Phycology. Almeria, Spain, pp. 1-19.

IPCC (2001) Climate Change 2001: The Scientific Basis. *In* Contribution of Working Group I to the Third Assessment Report of the Intergovernmental Panel on Climate Change, J.T. Houghton, Y. Ding, D.J. Griggs, M. Noguer, P.J. van der Linden, X. Dai, K. Maskell, and C.A. Johnson (Eds.). Cambridge University Press, Cambridge, United Kingdom and New York, pp. 881.

Iyengar, M.O.P. and Desikachary, T.V. (1981) Volvocales. Indian Council of Agricultural Research, New Delhi, India, pp. 374.

Kim, S.H. and Edmonds, J.A. (2000) Potential for Advanced Carbon Capture and Sequestration Technologies in a Climate Constrained World. PNNL-13095. Pacific Northwest National Laboratory, pp. 1-51.

Kobayashi, M., Kakizono, T., and Nagai, S. (1991) Astaxanthin production by a green alga *Haematococcus pluvialis* accompanied with morphological changes in acetate media. *Journal of Fermentation and Bioengineering* 71(5): 335-339.

Kobayashi, M., Kurimura, Y., Kakizono, T., Nishio, N., and Tsuji, Y. (1997) Morphological changes in the life cycle of the green alga *Haematococcus pluvialis*. *Journal of Fermentation and Bioengineering* 84(1): 94-97.

Law, A.M. and McComas, M.G. (2001) How to build valid and credible simulation models. *In* Proceedings of the 2001 Winter Simulation Conference, B.A. Peters, J.S. Smith, D.J. Medeiros, and M.W. Rohrer (Eds.). Arlington, Virginia, pp. 22-29.

Leung, P.S., Hochman, E., Wanitprapha, K., Shang, Y.C., and Wang, J.K. (1989) Optimal harvest schedule for maricultured shrimp: a stochastic sequential decision model. Research Series 060. College of Tropical Agriculture and Human Resources, Honolulu, Hawai'i, pp. 2-3.

LOICZ IGBP (2000) Stoichiometric analysis of CNP budgets. <http://data.ecology.su.se/MNODE/Methods/stoich.htm>. 28 September 2004.

Lorenz, R.T. and Cysewski, G.R. (2000) Commercial potential for *Haematococcus* microalgae as a natural source of astaxanthin. *Trends in Biotechnology* 18(4): 160-167.

Margalith, P.Z. (1999) Production of ketocarotenoids by microalgae. *Applied Microbiology and Biotechnology* 51(4): 431-438.

Masutani, S.M. and Nakamura, T. (1999) Review and analysis of Japanese CO₂ disposal research programs: final report. U.S. Department of Energy Order No. DE-AF26-98FT00720. Federal Energy Technology Center, pp. 1-72.

Mera Pharmaceuticals, Inc. (2003a) Aquasearch business overview. <http://www.aquasearch.com/business.htm#platform>. 3 February 2003.

Mera Pharmaceuticals, Inc. (2003b) Aquasearch technology and markets: overview. <http://www.aquasearch.com/technology.htm>. 3 February 2003.

Mera Pharmaceuticals, Inc. (2004) AstaFactor: astaxanthin and health. <http://www.astafactor.com/health.htm>. 11 September 2004.

Millero, F.J. (1979) The thermodynamics of the carbonate system in seawater. *Geochimica et Cosmochimica Acta* 43: 1651-1661.

Molina Grima, E., Acién Fernández, F.G., García Camacho, F., and Christi, Y. (1999) Photobioreactors: light regime, mass transfer, and scaleup. *Journal of Biotechnology* 70(1-3): 231-247.

Molina Grima, E., Fernández Sevilla, J.M., Sánchez Pérez, J.A., and García Camacho, F. (1996) A study on simultaneous photolimitation and photoinhibition in dense microalgal cultures taking into account incident and averaged irradiances. *Journal of Biotechnology* 45(1): 59-69.

Nakamura, T. and Senior, C.L. (2001) Recovery and sequestration of CO₂ from stationary combustion systems by photosynthesis of microalgae: quarterly technical progress report for the period ending 31 March 2001. U.S. Department of Energy Contract No. DE-FC26-00NT40934. National Energy Technology Laboratory, pp. 1-21.

Nakamura, T., Olaizola, M., and Masutani, S.M. (2004) Recovery and sequestration of CO₂ from stationary combustion systems by photosynthesis of microalgae: quarterly technical progress report #14. U.S. Department of Energy Contract No. DE-FC26-00NT40934. National Energy Technology Laboratory, pp. 1-23.

Olaizola, M. (2000) Commercial production of astaxanthin from *Haematococcus pluvialis* using 25,000-liter outdoor photobioreactors. *Journal of Applied Phycology* 12(3-5): 499-506.

Olaizola, M. (2004) Microalgal removal of CO₂ from flue gases: Effects of culture pH and flue gas composition on the efficiency of CO₂ capture. Manuscript submitted to *Energy Conversion and Management*.

Palumbo, A.V., McCarthy, J.F., Amonette, J.E., Fisher, L.S., Wulschleger, S.D., and Daniels, W.L. (2004) Prospects for enhancing carbon sequestration and reclamation of degraded lands with fossil-fuel combustion by-products. *Advances in Environmental Research* 8: 425-438.

Pruvost, J., Legrand, J., Legentilhomme, P., and Muller-Feuga, A. (2002) Simulation of microalgae growth in limiting light conditions: flow effect. *AIChE Journal* 48(5): 1109-1120.

Ramanathan, R. (1999) Selection of appropriate greenhouse gas mitigation options. *Global Environmental Change* 9(3): 203-210.

Rice, S.K., Brown, G.E. and Willing, R.P. (2002) Computer simulation modeling using STELLA to enhance investigative learning in a biology curriculum: what is STELLA. http://www1.union.edu/~rices/STELLA/stella_intro.html. 12 September 2004.

UNESCO (1987) Thermodynamics of the carbon dioxide system in seawater. *Technical Papers in Marine Science*. Paris, France, pp. 51.

U.S. Climate Action Network (1996) What is new about global warming in Florida? <http://www.climateactionnetwork.org/uscanweb/wnfl.pdf>. 22 September 2004.

U.S. Department of Energy (2004) Carbon sequestration r&d overview. <http://www.fe.doe.gov/programs/sequestration/overview.html>. 7 November 2004.

Weissman, J.C., Goebel, R.P., and Benemann, J.R. (1988) Photobioreactor design: mixing, carbon utilization, and oxygen accumulation. *Biotechnology and Bioengineering* 31: 336-344.

Wuebbles, D.J., Jain, A., Edmonds, J., Harvey, D., Hayhoe, K. (1999) Global change: state of the science. *Environmental Pollution* 100: 57-86.

Zonneveld, C. (1996) Modelling the kinetics of non-limiting nutrients in microalgae. *Journal of Marine Systems* 9(1-2): 121-136.